University of Missouri-Rolla
Electromagnetic Compatibility Laboratory

Title: Investigation of Fundamental Mechanisms Leading to Common-mode radiation from Printed Circuit Boards

Report Number: TR93-5-025R

Author: J.L. Drewniak
T. H. Hubing
T.P. Van Doren

Date: May 17, 1993

FINAL REPORT:
Investigation of Fundamental Mechanisms Leading to Common-mode Radiation from Printed Circuit Boards

Prepared for
General Motors
as part of Purchase Order PGS21122

J. L. Drewniak, T. H. Hubing, and T. P. Van Doren

Electromagnetic Compatibility Laboratory
Department of Electrical Engineering
University of Missouri-Rolla
Rolla, MO 65401

May 17, 1993

Contents

Abstract

Radiation from printed circuit designs is of serious concern to many industrial and government organizations. EMC engineers are well aware of radiation problems with printed circuit designs, and considerable effort is expended to determine and eliminate the source of these problems. There is, however, an incomplete knowledge of the fundamental mechanisms by which differential-mode sources produce or induce common-mode currents, and the resulting common-mode radiation. This incomplete knowledge leads to a trial-and-error approach to solving common-mode radiation problems that can be very time-consuming. The investigation reported herein has focussed on determining the underlying physics of common-mode radiation. A more complete understanding of the mechanisms that lead to common-mode radiation will enable EMC engineers to more easily determine the source of the problem and thereby the solution. Two fundamental mechanisms have been identified, one associated with a differential-mode voltage that results in a common-mode current on a cable bundle attached to a printed circuit board, and the other associated with a differential-mode current resulting in common-mode current on the cable. The two mechanisms are demonstrated through numerical and experimental studies. Techniques and strategies are presented, based on the results of the investigation, to assist EMC engineers in determining and eliminating sources of common-mode radiation in typical printed circuit designs.

1 Introduction

Radiation from digital circuits is of significant concern to designers and manufacturers of products incorporating electronic components. The FCC and other trade and regulatory bodies place stringent regulations on unintentional radiation from electronic systems. Further, radiated emissions are a significant source of interference affecting the self compatibility of many systems. Electromagnetic compatibility (EMC) engineers and circuit designers are well aware of this problem, and possess a wealth of knowledge on many aspects of radiation from high-speed printed circuit designs. This accumulated knowledge is a result of years of experience and observations in producing designs that seek to minimize radiated emissions. However, as technology advances in the direction of faster digital electronics, and higher density designs, difficulties with radiation from digital circuits become increasingly problematic. While a great deal of experimental knowledge exists, there is yet an incomplete understanding of the fundamental mechanisms that produce common-mode radiation from a printed circuit design. The objective of the study reported herein was to investigate and determine fundamental mechanisms by which differential-mode signals produce common-mode currents on an attached cable bundle, with the resulting radiation. The goal is a more complete understanding from which general design techniques for minimizing common-mode radiation can be determined, as well as providing direction in determining and eliminating common-mode radiation from existing designs. Since EMC engineers as well as circuit designers possess a sound understanding of differential-mode radiation, and are well versed in techniques to minimize this type of radiation, this investigation has focused on common-mode radiation.

One perspective from which to view radiation is simply as a source driving an antenna. While common-mode current is a mathematical quantity, and often cannot be assigned to a single conductor, it is conceptually useful for understanding common-mode radiation to think of the common-mode current as existing on an equivalent "antenna" conductor. Common-mode "antennas" will be referred to in this sense throughout the report. In the case of common-mode radiation, the antenna consists of the conductors on which the common-mode current exists. These typically include conductors that extend well beyond the conductors on the printed circuit board carrying differential-mode currents. One example is the Daytime Running Lamp module discussed in detail in Section 3.2. In this case the common-mode antenna consists of the I/O lines attached to the printed circuit board, and the considerable conductor area of several on-board relays. The common-mode source is the equivalent voltage or current source that drives the common-mode antenna. The driving source is often a secondary source that results from a differential-mode current or voltage. The common-mode source may result from differential-mode signals, or as in the case of

delta-I noise on the DC power bus, may result from differential-mode noise. The first objective of this study was to investigate the mechanisms by which the primary differential-mode voltages and currents produce or induce secondary common-mode sources that drive common-mode antennas, as well as determine the manner in which common-mode antennas might arise in the course of a typical printed circuit design. Second, the effect of design choices such as circuit layout, components, etc., on the common-mode antennas and driving sources was studied.

As stated above, EMC engineers and circuit designers are well versed in techniques for minimizing differential-mode radiation. In the case of differential-mode radiation, the antenna is comprised of the conductors on which the differential-mode currents (typically signal currents) exist. These antennas are easily determined simply by tracing the signal path. Differential-mode radiation is typically minimized by maintaining small signal loop areas. In designs where signal loop areas are kept small, the primary contributions to radiated emissions then come from common-mode current, even though the differential-mode current may be orders of magnitude greater than the common-mode current. An example is given by Paul [1]. A differential-mode current of 20 mA in a 1 m length of ribbon cable with a wire separation of 50 $mils$, will produce radiated emissions of 40 $\frac{dB\mu V}{m}$ at a distance of 3 m, while only 8 μA of common-mode current is required to produce the same field. A useful analogy for differential-mode and common-mode current in parallel, closely spaced conductors is the folded dipole antenna. The radiation and input impedance of a folded dipole is typically determined by decomposing the currents on the antenna into transmission line currents and antenna currents [2]. The antenna currents are the radiating currents, and the transmission-line currents non-radiating. Differential-mode currents are analogous to the transmission-line currents, and common-mode currents analogous to the antenna currents.

While EMC engineers have been aware of common-mode radiation for some time, studies of common-mode radiation reported in the open literature have been few, and have appeared only relatively recently. Paul has emphasized the need to consider and model common-mode currents in order to adequately predict radiation from printed circuit designs [3], [4]. Simple battery powered test circuits employing a single oscillator and attached leads were constructed to show that the resulting radiation could not be predicted by differential-mode currents alone. Hubing and Kaufman investigated radiation from electrically small table-top products [5], [6]. Numerical (method of moments) and experimental studies were reported for wire circuit models driven by a voltage source. One meter long cables were attached to different wire circuit configurations. The currents resulting in the circuit and attached cable were decomposed into uniform and nonuniform components corresponding to differential- and common-mode, and the resulting radiation calculated.

The study proposed an *end driven wire* modeling technique for reducing the modeling of common-mode radiation to only those features that were significant to the problem. Hardin et al. recently reported a study on the prediction of common-mode radiation [7]. The method of moments was employed to numerically model simple asymmetric wire circuit geometries. The wire geometries were decomposed into symmetric and asymmetric configurations, and the common-mode current and common-mode radiation determined from the asymmetric model. Good agreement was obtained between the experimental and numerical results. A numerical study employing the method of moments of radiation from printed circuit boards has also been reported [8]. The study applies the method of moments to the two simple problems of radiation from a signal loop (differential mode) on a printed circuit board, and a long wire attached to a printed circuit board (common mode). Test configurations were constructed and measurements of current were obtained, and in general agreed well with the numerical results. While these studies have been confined to modeling very simple structures, efforts continue in the attempt to model and predict common-mode radiation from the significantly more complex geometries typically encountered in printed circuit designs. A recent study by Hubing notes that these models and techniques must properly include features that will allow prediction of common-mode currents [9]. Attempting to predict radiation from printed circuit designs with techniques that compute only differential-mode currents, or eliminating geometric features that contribute to the common-mode radiation, will result in poor agreement between the models and the measured radiation.

Numerical and experimental results of an investigation of common-mode current in printed circuit geometries are reported herein. Fundamental mechanisms of common-mode radiation are discussed in Section 2. General properties of wire-type antennas are discussed briefly. Two fundamental mechanisms have been identified by which differential-mode signals and noise can result in common-mode current. These mechanisms are illustrated in Section 2 with simple wire circuit geometries. Results of numerical full-wave simulations for wire circuit geometries are presented to illustrate the two mechanisms. Transfer impedance concepts are presented that relate differential-mode currents and voltages to the common-mode current producing the radiation. Experimental results of the study are presented in Section 3, and details of the measurement systems and procedures are given. Results of a susceptibility example will be discussed as an illustration of a case where a transfer impedance can be derived that relates a common-mode current to a differential mode voltage. The transfer impedance is given as a function of the circuit geometry. Results of four simple passive circuit geometries that are representative of printed circuit configurations are given. The differential-mode driving source for the circuit configurations is provided by a network analyzer. Finally, experimental results for the Daytime Running Lamp (DRL) module provided

by General Motors are presented. The results clearly illustrate the two identified mechanisms, though one is found to dominate the measured common-mode current. Strategies and techniques to assist EMC engineers in determining the source of a common-mode radiation problem are given in Section 4.

2 Fundamental Mechanisms of Common-mode Radiation

2.1 "Antennas"

Fundamentally, radiation requires an antenna with a driving source. If either of these components of the radiating system is eliminated, or if the source is decoupled from the antenna, the entire system is an ineffective radiator. Eliminating or minimizing common-mode radiation from printed circuit designs then becomes a problem of identifying potential common-mode driving sources and antennas, and rendering one or the other ineffective through a judicious choice of related design features. Throughout this report, the conductors on which common-mode current exists, and from which common-mode radiation is produced, are referred to as antennas, or common-mode antennas. The antennas of particular concern in this study are of the "wire-type", i.e., antennas with two distinct conductor halves at different RF potentials that are driven against each other producing the radiation. As discussed above, there are circuit configurations that result in radiation from loop-type antennas, however, small loops are ineffective radiators, and loops large enough to present a problem are usually easy to identify and eliminate. Since the power radiated by a wire antenna is given by (neglecting ohmic losses)

$$P_r = \frac{1}{2} \mid I_{in} \mid^2 \; Re\{Z_{in}\}$$

the radiated power can be decreased if either the input current or the input resistance $R_{in} = Re\{Z_{in}\}$ is decreased. In many practical design cases where the effective antenna is short, the input impedance is primarily reactive and therefore the input resistance is small (but nonzero). The radiated power is therefore more easily reduced by reducing the input current. This can be accomplished by increasing the input reactance. It is useful to observe the variation in the input impedance for the different types of wire dipole antennas shown in Figure 1. In the case where the wire dipole antennas are center-fed, the current maximum occurs at the feed point (for frequencies below the half-wavelength resonance). For short antennas where $\frac{\ell}{\lambda} << 1$, the current distribution is triangular, and the input impedance is dominated by the reactance

$$\mid Z_{in} \mid = \mid \frac{V}{I_{in}} \mid \approx \frac{1}{\omega C}$$

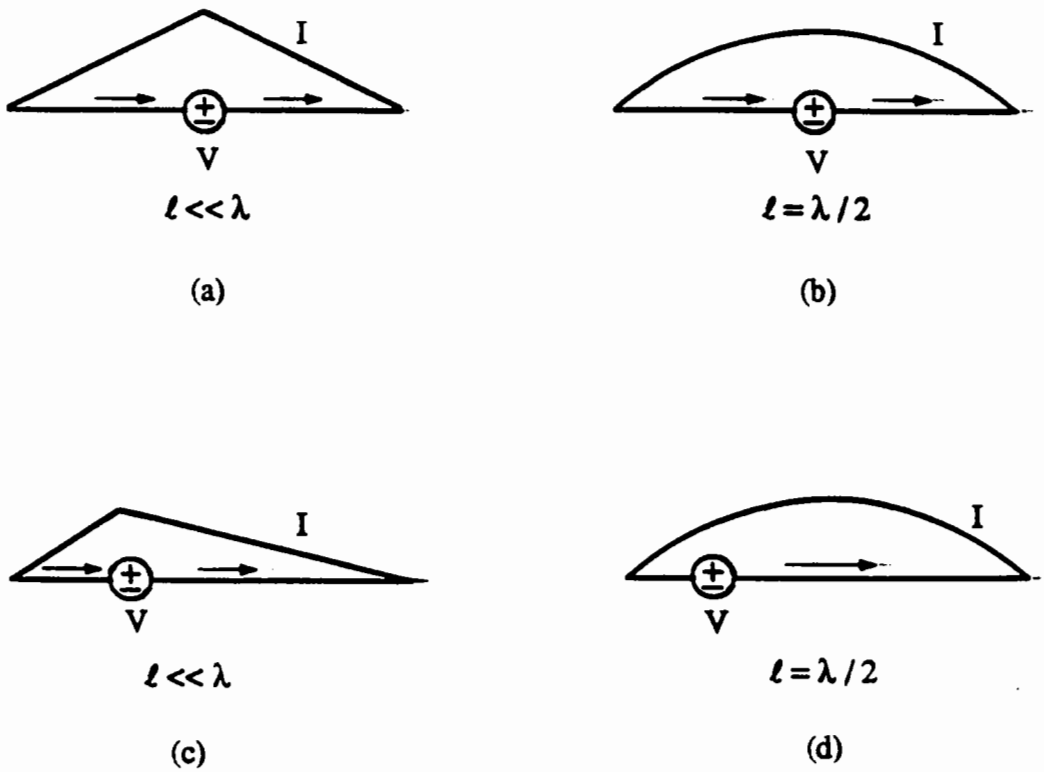

Figure 1: Current distribution and input impedance for dipole antennas. a) short, center-fed dipole, b) half-wavelength, center-fed dipole, c) short, off center-feed dipole, d) half-wavelength, off center-feed dipole.

and is very large. The current distribution on a center-fed half-wave dipole is nearly sinusoidal with the current maximum occurring at the input as illustrated in Figure 1(b). The input impedance is real and $Z_{in} = 73\ \Omega$. Wire antennas that are not center fed are shown in Figures 1 (c) and (d). For a short antenna, the current is again a maximum at the feed point, however, the input impedance is much larger than in the center-fed case. The input impedance of a half-wave dipole fed off-center is given by

$$Z_{in} = \frac{73}{cos^2 \beta d}\ \Omega$$

where $\beta = \frac{2\pi}{\lambda}$, and d is the displacement of the feed from the antenna midpoint. As in the case for a center-fed dipole, the current peaks at the center of the antenna. However, the input impedance increases rapidly as the feed is displaced from the center of the antenna, becoming infinite when $d = \frac{\lambda}{4}$, or the feed is at the end of the antenna.

The behavior of the input impedance for short and half-wavelength dipole antennas provides some insight into configurations that are desirable and undesirable in the design of printed circuits with attached cables. The effectiveness of ferrite loading of an antenna can also be seen from this behavior. First, it is clear that if potential radiating structures on a printed circuit design are fed near one end, the input impedance will be very large. Then, the input current for a given driving voltage will be small for short and half-wavelength antennas, and the resulting common-mode radiation will be small. The worst case is a half-wave dipole fed at the center of the antenna. Second, if the antenna is short, and/or fed near one end where the magnitude of the input impedance may be several hundred to several thousand ohms, adding series loading of $50 - 100\ \Omega$, as with a ferrite sleeve, will achieve little in reducing the input current to the antenna, and hence the common-mode radiation. In certain practical circuit design configurations, at least one half of the antenna is often easily identified. For example, a wiring harness of significant length relative to the measured EMI harmonic component, is often one half of a relatively effective antenna. The other half of the antenna is often more difficult to determine, and will depend upon the source mechanism driving the antenna.

2.2 Driving Sources

Two fundamental source mechanisms have been identified. These source mechanisms have been denoted *voltage* and *current* mechanisms to distinguish the differential-mode quantity that provides the driving source of the common-mode current on the radiator. A wire circuit example that illustrates the physics of the current driven mechanism is shown in Figure 2 (a). An ideal voltage source is shown, so that the current is limited entirely by the inductance of the shorted loop. If the

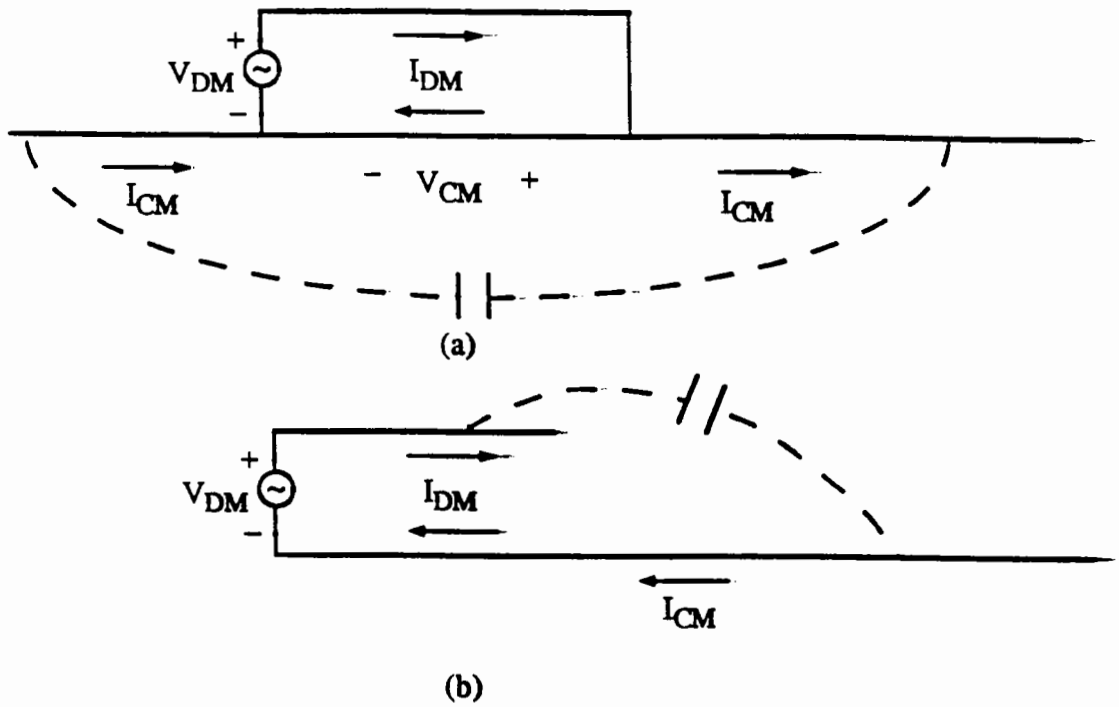

Figure 2: Wire circuit examples illustrating the physics of the a) current and b) voltage driven mechanisms.

loop inductance is decomposed into partial inductances for the upper and lower conductors [1], [10] (assuming the vertical branches contribute negligibly small partial inductance), the large differential mode current through the partial inductance of the lower conductor results in a voltage drop. This voltage drop provides a common-mode voltage source that can drive common-mode current on the extended lower conductor as shown. An equivalent alternative perspective to partial inductance, which is useful in developing transfer impedance concepts to relate the differential-mode quantities to common-mode current, is the the mutual inductance between the differential-mode loop and the common-mode loop. Partial inductance is discussed in more detail in the appendix. The voltage developed along the lower conductor over the length of the differential-mode loop is then $V_{CM} = j\omega M$, where M is the mutual inductance. An example of the current driven mechanism occurring in a printed circuit design is the differential-mode noise current drawn by a switching gate from a decoupling capacitor. In a single layer design, large switching currents are drawn through the loop, inducing a noise voltage drop on the ground (reference) conductor. Any extended portions of the reference conductor can then act as an antenna that is driven by this source. Experimental results for this particular example will be shown for the DRL module (though the current driven mechanism is dominated in this case by the voltage driven mechanism).

A wire circuit example illustrating the voltage driven mechanism is shown in Figure 2 (b). In this case the differential-mode voltage provides the driving source that results in common-mode current. A description of the physics of the common-mode radiation is facilitated by the use of static flux mapping techniques. The potential difference between the lower and upper conductors results in equal and opposite charge residing on the conductors. The charge is distributed over the length of the conductor on both the upper and lower conductors. The corresponding flux map then has some flux lines that originate on the positively charged upper conductor, and terminate on the extended portion of the lower conductor. For time varying sources, the charge distribution varies with time, and the time rate of change of the charge distribution is the common-mode current. A circuit illustration of this is indicated by the capacitor in Figure 2 (b). The imbalance or asymmetry then results in common-mode current in the circuit, producing common-mode radiation. A differential-mode voltage provides the driving source for the antenna, and might include signals, or differential-mode noise such as on the DC power distribution bus. The input impedance of the antenna is related to the extent of the two conductor halves. One half of the antenna might typically be the ground (reference) conductor, which can have a significant extent due to grounded cables, shields, and enclosures connected to the printed circuit board. The other half of the antenna must be of sufficient extent to provide a small enough input impedance to result in significant common-mode current. In the case of signal traces, the other half of the antenna is often too limited in extent to provide a sufficiently low antenna input impedance for the source to drive. There will be, however, practical design examples where the two halves of an antenna are of sufficient extent for the differential-mode voltage source to drive them effectively. Another possibility for producing common-mode current on an attached cable bundle from a voltage driven mechanism is imbalance in the I/O cable, and/or the loads attached to the cable. In this case both "antenna halves" are effectively in the cable bundle.

Numerical and experimental studies reported by Hardin, Paul, and Naishadham have demonstrated that asymmetries or imbalances in circuit geometries can lead to common-mode radiation [7]. However, discerning the asymmetry may not always be straight-forward, in particular for the current driven mechanism. It is thus useful to relate the parameters of the circuit geometry to the common-mode current that produces the radiation. For the current driven mechanism, it is desired to relate the differential-mode quantity (current) to the common-mode current produced on an attached cable. A relation for the ratio of the differential-mode current to the common-mode current is given by

$$\frac{I_{DM}}{I_{CM}} = \frac{I_{DM}}{V_{CM}} \frac{V_{CM}}{I_{CM}} = \frac{Z_{in}}{Z^{I}_{transfer}}$$

where

$$Z^I_{transfer} \triangleq \frac{V_{CM}}{I_{DM}}$$
$$Z_{in} = \frac{V_{CM}}{I_{CM}}$$

$Z^I_{transfer}$ is defined as the transfer impedance for the current driven mechanism, and Z_{in} is the input impedance to the antenna driven by the equivalent common-mode driving source. The transfer impedance can be related directly to the mutual inductance M described above

$$Z^I_{transfer} = j\omega M$$

A transfer impedance may also be defined for the voltage driven mechanism as

$$Z^V_{transfer} \triangleq \frac{V_{DM}}{I_{CM}} = \frac{1}{j\omega C}$$

where the capacitance C will be a function of the circuit geometry.

2.3 Numerical Results

Numerical simulations on simple wire circuit configurations were conducted to test the physics described above. The circuit configurations are shown in Figure 3. The simulations were performed using the Numerical Electromagnetics Code (NEC) [11]. NEC is a proven full-wave electromagnetic modeling code based on the method of moments that has been found to be superior for wire geometries. While the circuits that were investigated are simple, they are representative of the wire-type antennas that typically arise with common-mode radiation problems in printed circuit designs. In each case the source frequency is 30 MHz, and the source voltage is 1 V. In Figures 3 (a) and (b) the geometries are short in terms of the free-space wavelength which is 10 m. The wire radius in each circuit is 0.8 mm. The common-mode current was computed simply by subtracting the current on the upper conductor from that on the lower conductor [1]. The common-mode current for an open circuit ($Z_L = \infty$) case of Figure 3 (a) is shown in Figure 4 (a). The driving source for the common-mode antenna is V_{DM}, and the extent of the two halves of the conductor is sufficient to result in a significant common-mode current, with a peak current of 120 μA. In this case the common-mode current is a result of the differential-mode voltage source. This is an example of a voltage driven mechanism.

The current driven mechanism for the same wire circuit configuration of Figure 3 (a) results when the load impedance Z_L is small. Numerical results for the common-mode current for $Z_L = 0$

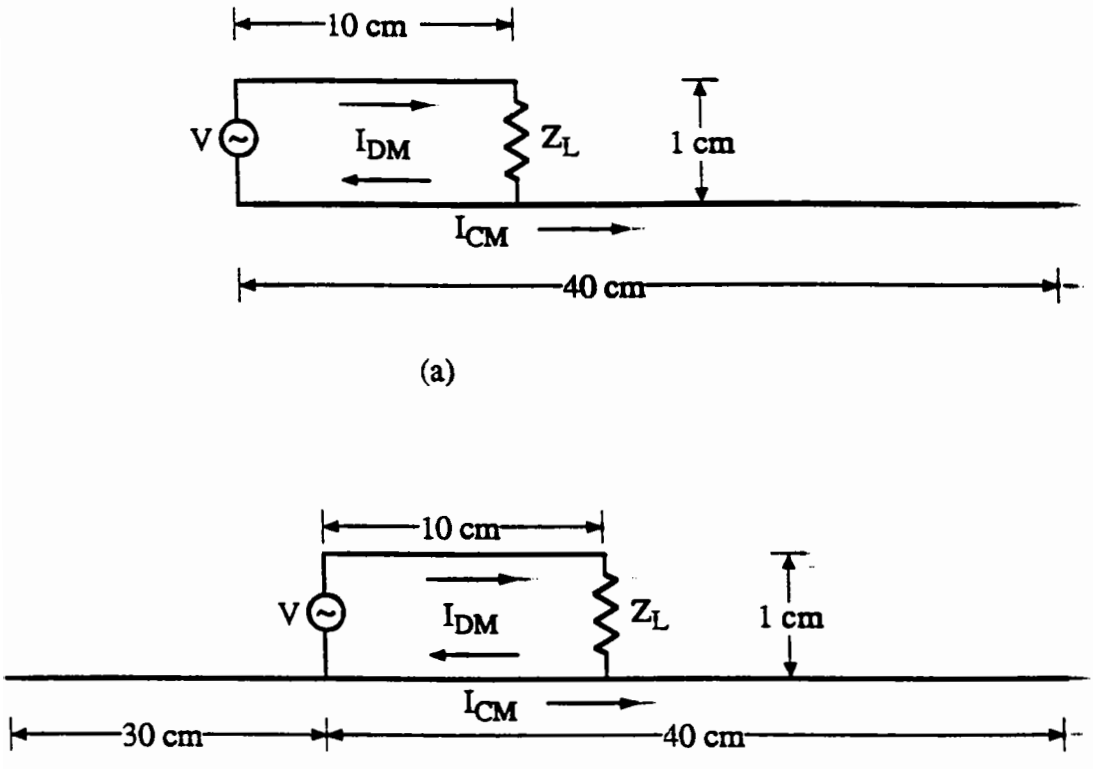

Figure 3: Representative wire circuit geometries investigated using NEC.

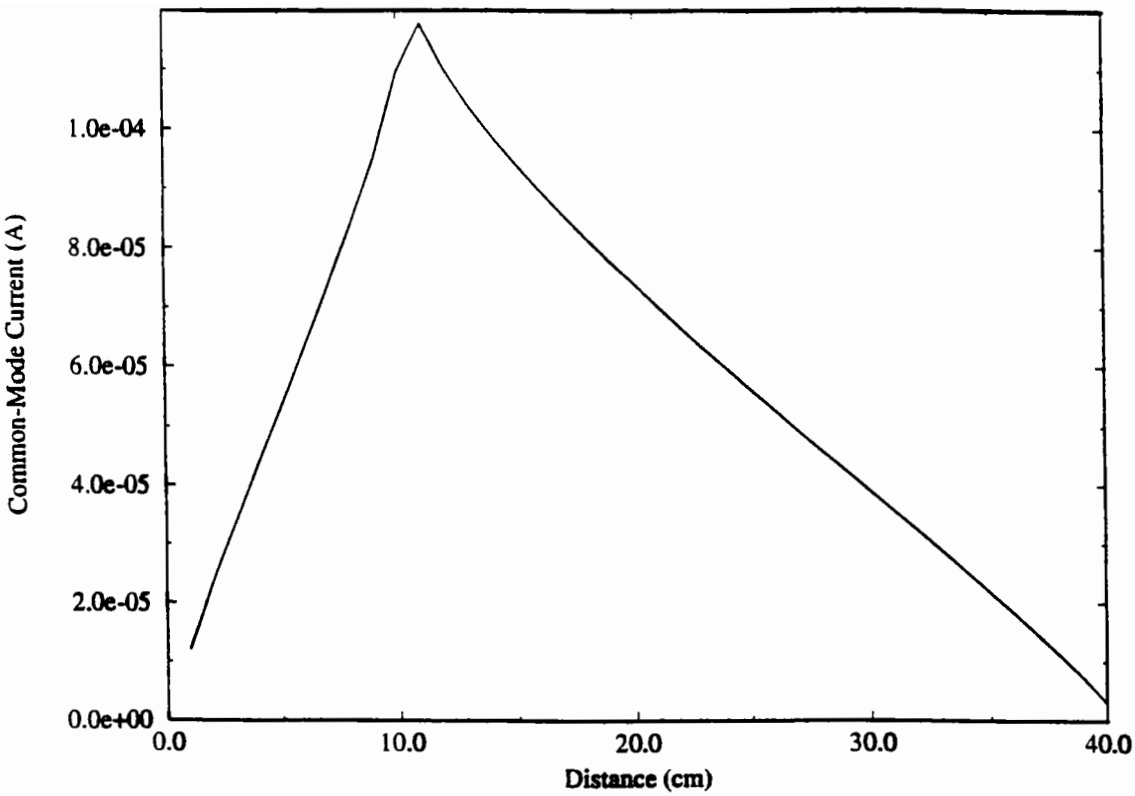

(a)

≃ 20dB difference

See measu in Figure

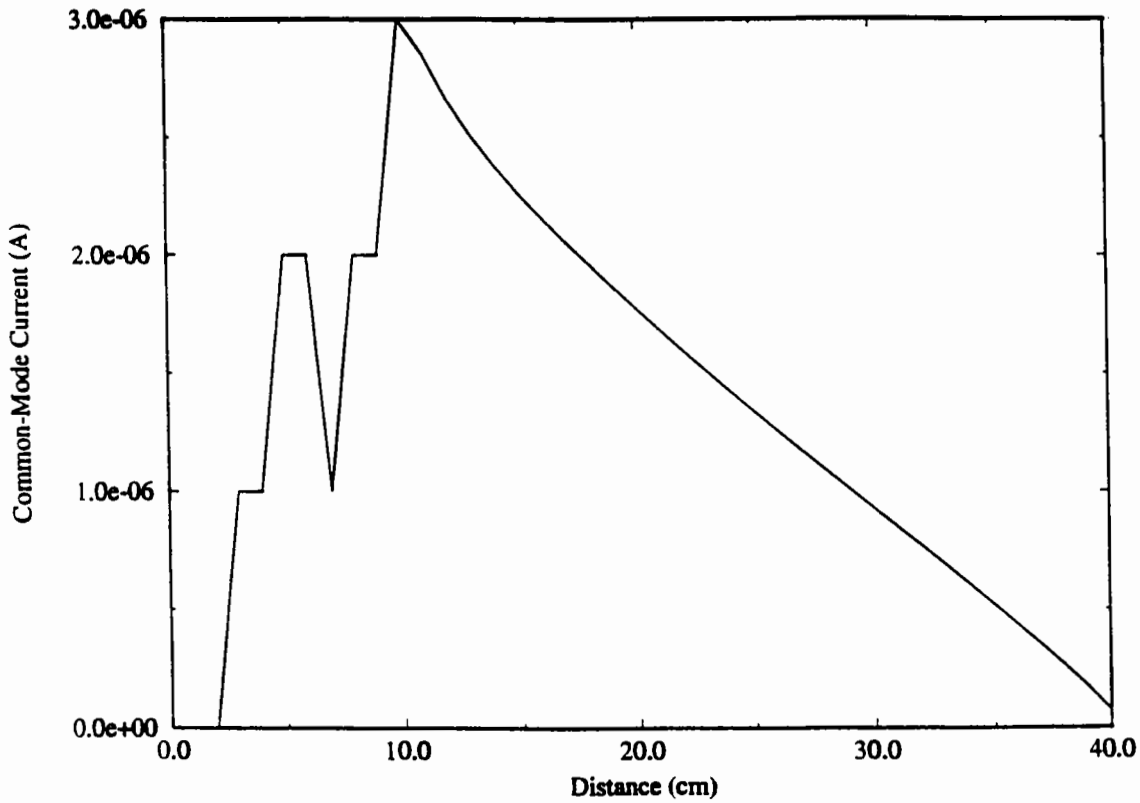

(b)

Figure 4: Common-mode current computed using NEC for a) open and b) short circuit cases of Figure 3 (a). The origin is the left-most point in the circuit.

are shown in Figure 4 (b). The jump discontinuities shown in the common-mode current are numerical artifacts. Too few significant figures in the NEC code were written to the output file, resulting in subtraction noise when computing the common-mode current. It is observed that the common-mode current is very small in this case, approximately 30 dB below that in the voltage driven case, even though the differential-mode current in the current driven case is more than two orders of magnitude greater than that in the voltage driven case. The large difference in the resulting common-mode currents is due to the antenna configuration which is driven by the equivalent common-mode source. In the voltage driven case, the source is $\frac{1}{2}V$, and is located on the antenna such that the wire-type antenna has two halves of sufficient extent to be an effective common-mode radiator. For the current driven mechanism, the equivalent common-mode source driving the antenna is a voltage source V_{CM} that is distributed over the length of the differential-loop portion of the lower conductor. The placement of the source with respect to the antenna is such that the antenna is effectively driven very near one end. The input impedance for a wire antenna driven near one end becomes very large, and hence, the common-mode current is significantly smaller than in the voltage driven case. The next example indicates that it is primarily the difference in the antenna input impedance that is the primary contributor to the significantly different common-mode current, and not the difference in the two equivalent common-mode driving sources.

A second example illustrating the physics of the voltage and current driven mechanisms is shown in Figure 3 (b). Numerical simulations employing NEC were performed with $Z_L = \infty$, and $Z_L = 0$, corresponding to the voltage and current driven mechanisms, respectively. The geometry and source parameters are the same as in the previous wire circuit examples, with the exception that the lower conductor is extended on the other side of the source by 30 cm as shown. The common-mode current that results for the voltage driven mechanism with $Z_L = \infty$ is shown in Figure 5 (a). The equivalent common-mode driving source is again provided by the differential-mode voltage source V. As can be observed, the common-mode current is in opposite directions on the two different sides of the symmetry plane of the wire. This is expected, since the capacitance between the upper conductor and each of the lower two halves results in current flowing in opposite directions on the lower conductor. The computed common-mode current on the right hand side of the lower conductor is less in this case than in the open-circuited configuration of Figure 3 (a). It is worth noting in this example, that although significant common-mode current results on the lower conductor, there are two distinct components of the current, one on each of the wire halves, and that these are equal in magnitude and oppositely directed. As far as the common-mode radiation is concerned it is expected that the radiation from these two currents will nearly cancel. Computed results of NEC for radiated power in this case was 0.035 nW, as compared to 2 nW for the open

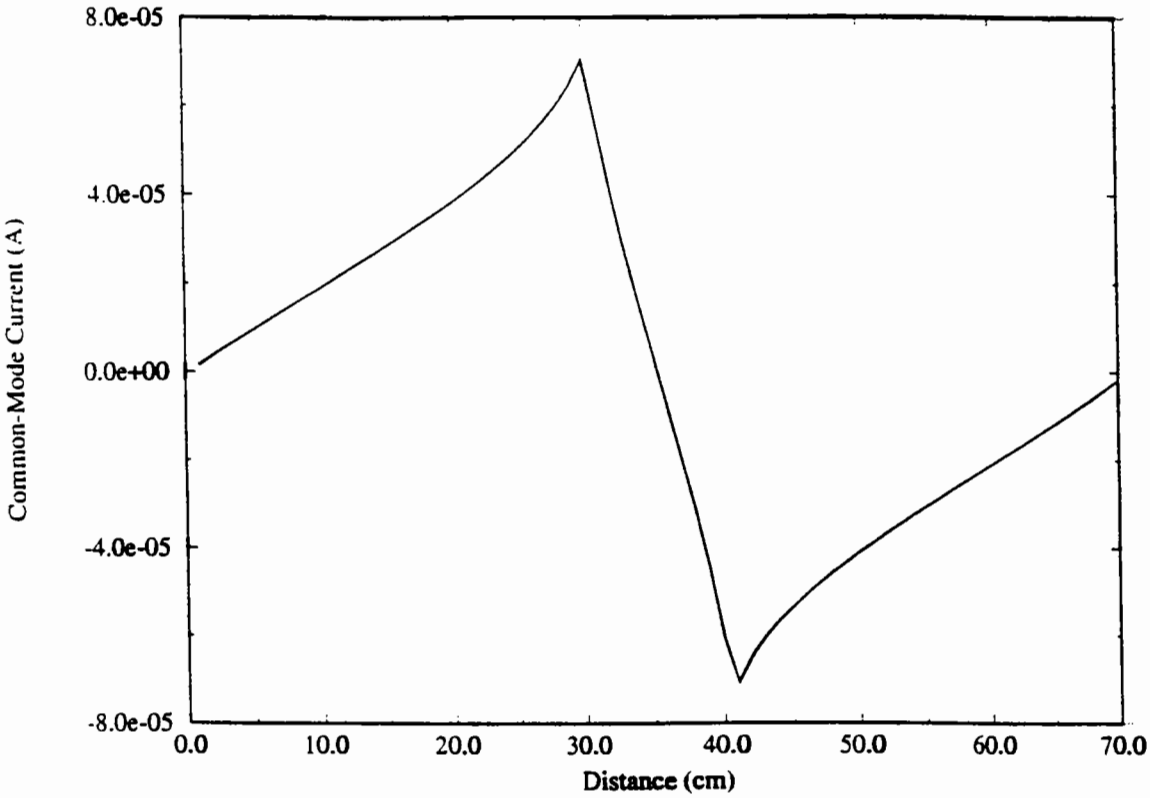

(a)

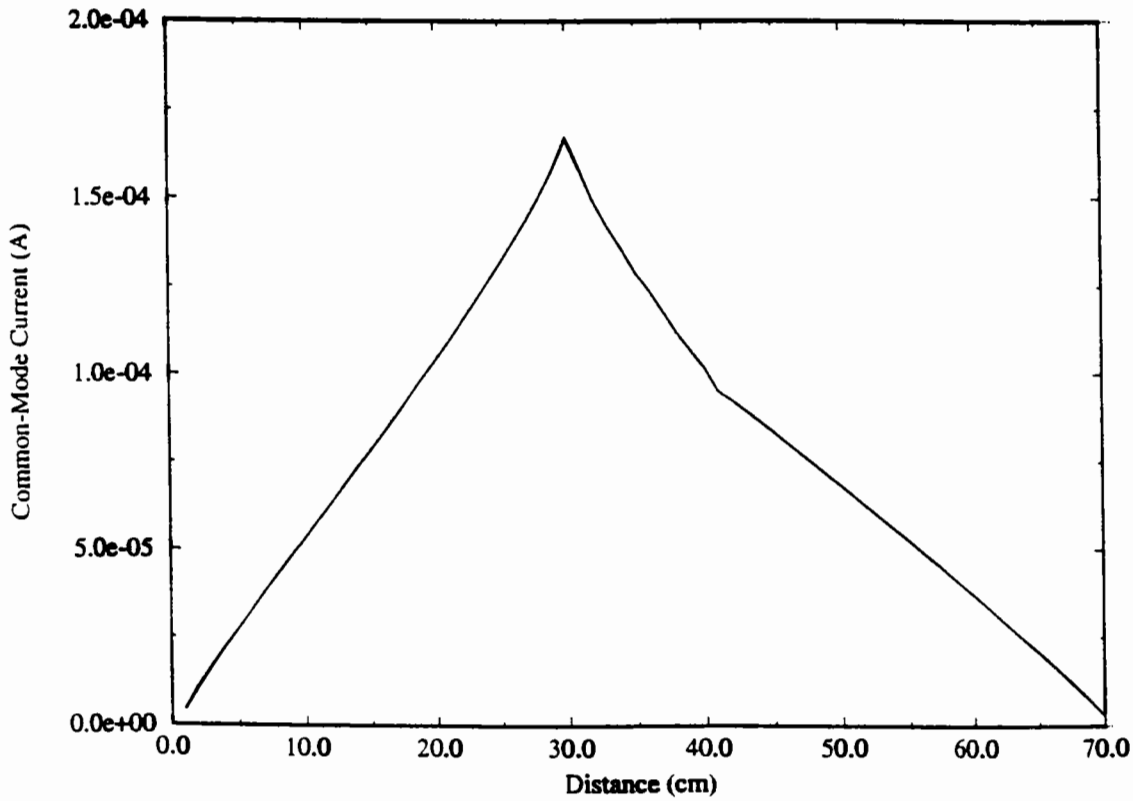

(b)

Figure 5: Common-mode current computed using NEC for a) open and b) short circuit cases of Figure 3 (b). The origin is taken to be the left-most point on the lower conductor.

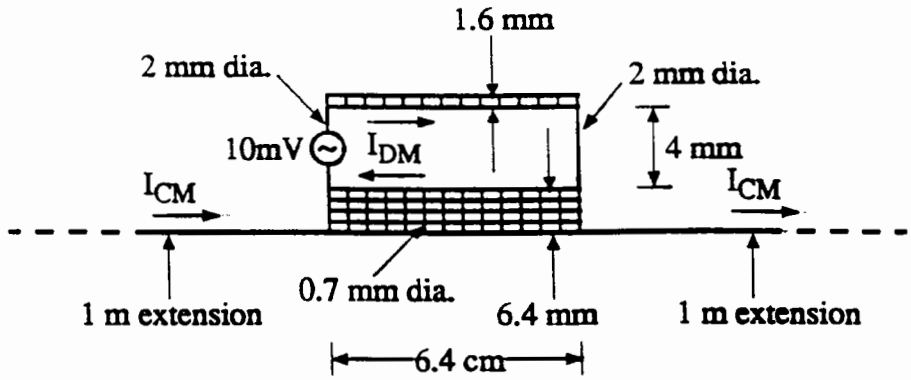

Figure 6: Circuit for NEC computations which approximates the current driven mechanism in the DRL module.

circuited case of Figure 3 (a).

The common-mode current computed for the current driven mechanism with $Z_L = 0$ for the wire circuit geometry of Figure 3 (b) is shown in Figure 5 (b). Again, the differential-mode current in the lower conductor branch of the differential-mode loop results in a voltage drop along this length. The voltage drop results in an equivalent common-mode voltage source that is distributed over the length of the conductor. This equivalent voltage source then drives the common-mode antenna, which is comprised of the two halves of the lower conductor. The differential-mode current in this case is essentially the same as for the previous geometry of Figure 3 (a) with $Z_L = 0$, however, the peak common-mode current is 35 dB greater. The common-mode current is observed to be asymmetric, and is a result of the distributed voltage source.

NEC simulations were also done for the circuit shown in Figure 6. The differential-mode loop geometry was chosen to approximate the source for the current driven mechanism in the DRL module with a decoupling capacitor at the connector. One meter wires are then attached to the differential-mode loop. The solid conductors of the DRL module printed circuit were approximated with a wire grid of similar dimensions. A 10 mV ideal voltage source is applied and the common-mode current on the attached wires is determined, as well as the maximum value of the electric field at 1 and 3 m, at 40, 50, and 60 MHz. The current at the source is nearly entirely imaginary, and is 3.8, 4.8, and 5.7 μA, at 40, 50, and 60 MHz, respectively. The maximum value of the electric field in the plane of the circuit and along the midpoint of the differential-mode loop at a distance of 1 m is 14.3, 20.3, and 28.7 $\frac{dB\,\mu V}{m}$, at 40, 50, 60 MHz, respectively. At a distance of 3 m the maximum electric field is 6.8, 13.7, and 22.1 $\frac{dB\,\mu V}{m}$, at 40, 50, and 60 MHz, respectively. The peak

value of the common-mode current was 11.1, 15.7, and 22.0 nA, at 40, 50, 60 MHz, respectively. These values are computed for a source of 10 mV, however, the results can be scaled for other source values.

3 Experimental Results

Several different test configurations were designed, constructed, and measurements obtained, in order to experimentally verify the two mechanisms described in the previous section. Both passive and active circuit geometries were tested.

3.1 Experimental Test Configurations

A susceptibility problem was studied to demonstrate the transfer impedance concept for relating common-mode and differential-mode quantities only as a function of geometry. A cross-sectional view of the test configuration is shown in Figure 7 (a). The width (unshown dimension) of the rectangular box was 8″. Measurements of $\mid S_{21} \mid$ were obtained with Port 1 of the network analyzer providing the source of the input common-mode current (the connector at the box gap). The primary loop was terminated in 50 Ω, and the secondary loop short circuited. The incident common-mode current produces a differential-mode voltage in the secondary loop. The ratio of the differential mode voltage to the common-mode current can be related to only geometric parameters by

$$Z_{transfer} \triangleq \frac{V_{DM}}{I_{CM}} = \frac{\omega \mu_o \ell h}{w}$$

where $\ell = 2''$ is the length of the secondary loop, $h = 0.1''$ is the height of the conductor in the secondary loop above the ground plane, and $w = 8''$ is the width of the box. The transfer impedance can be related to the measured $\mid S_{21} \mid$ by

$$\mid S_{21} \mid = 20 \; log \left[\frac{\omega \mu_o \ell h}{Z_o w} \right] \quad (dB)$$

if the input current is assumed to spread into a current sheet at the secondary loop, and the 50 Ω impedance of Port 2 results in negligible loading of the secondary loop. Measured results for $\mid S_{21} \mid$ are shown in Figure 7 (b). The results calculated using the above equation agree well with the measured results. At 10 MHz the calculated value is -54 dB, which is very close to the measured value. Calculated and measured values at 50 MHz and 100 MHz agree equally as well.

Test configurations to investigate the fundamental mechanisms of common-mode radiation described in the previous section were also constructed and measurements conducted. The HP8753C

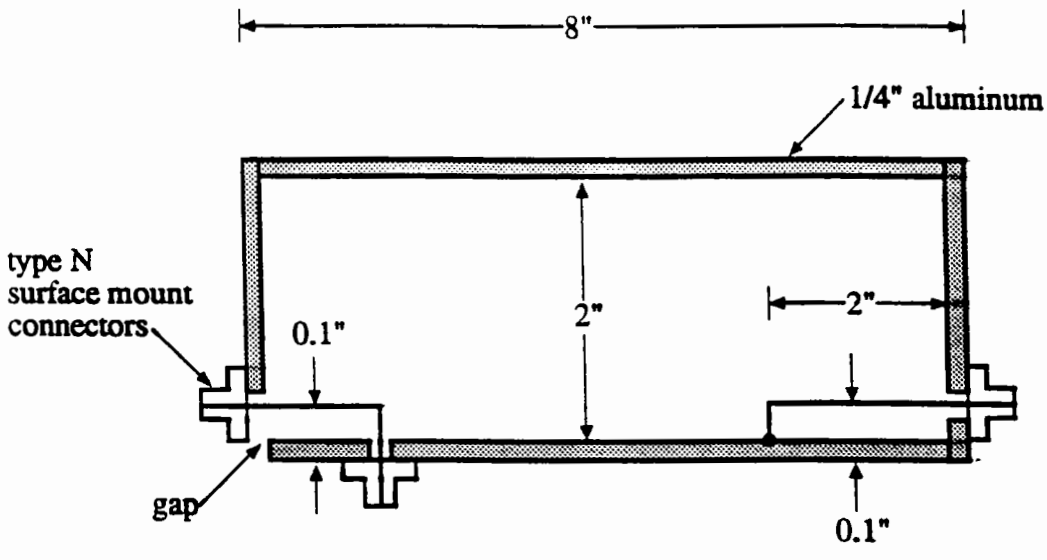

(a)

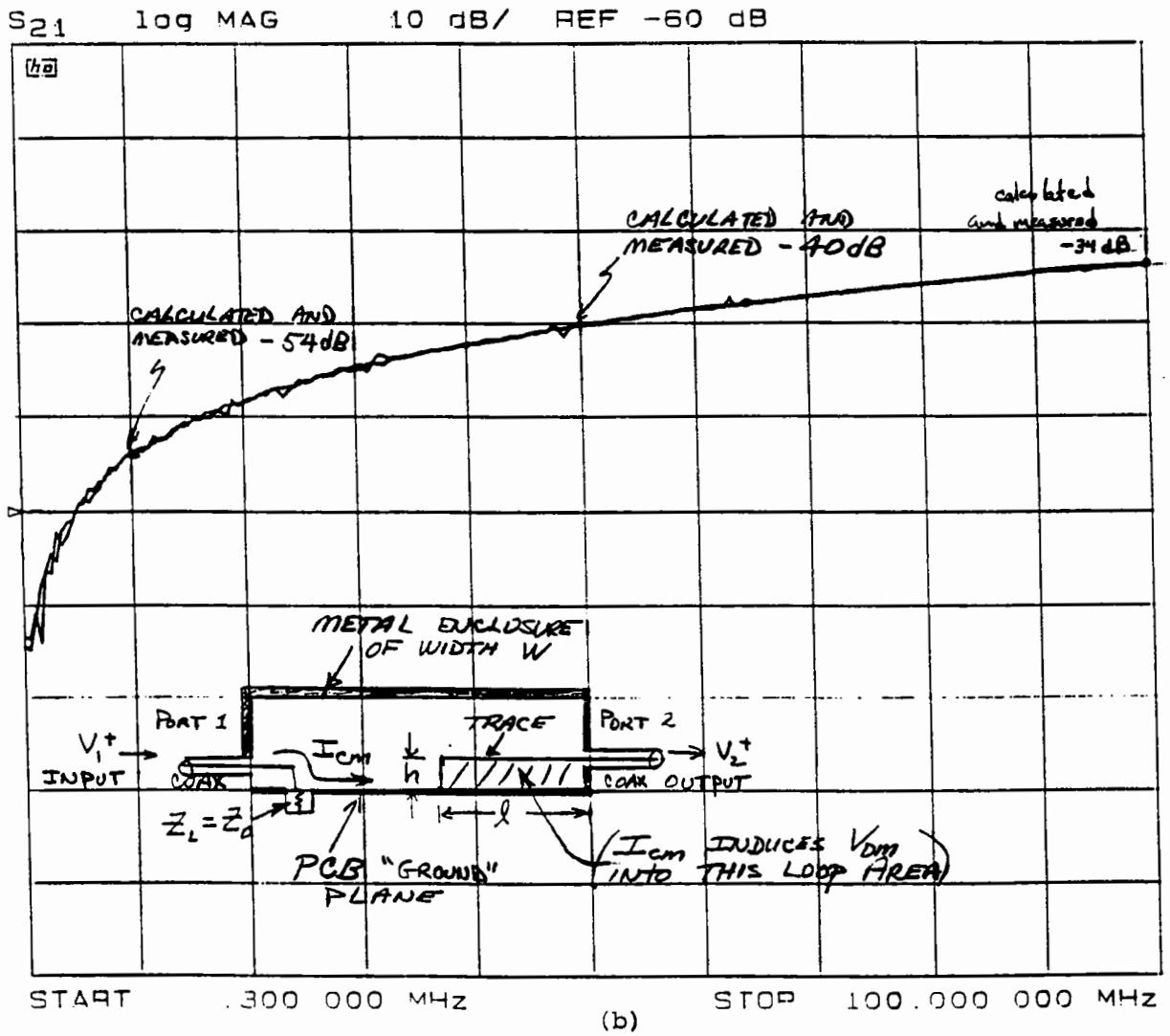

(b)

Figure 7: Susceptibility example to demonstrate transfer impedance concepts. a) Test configuration cross-sectional geometry, b) results for a 50 Ω load on the primary loop.

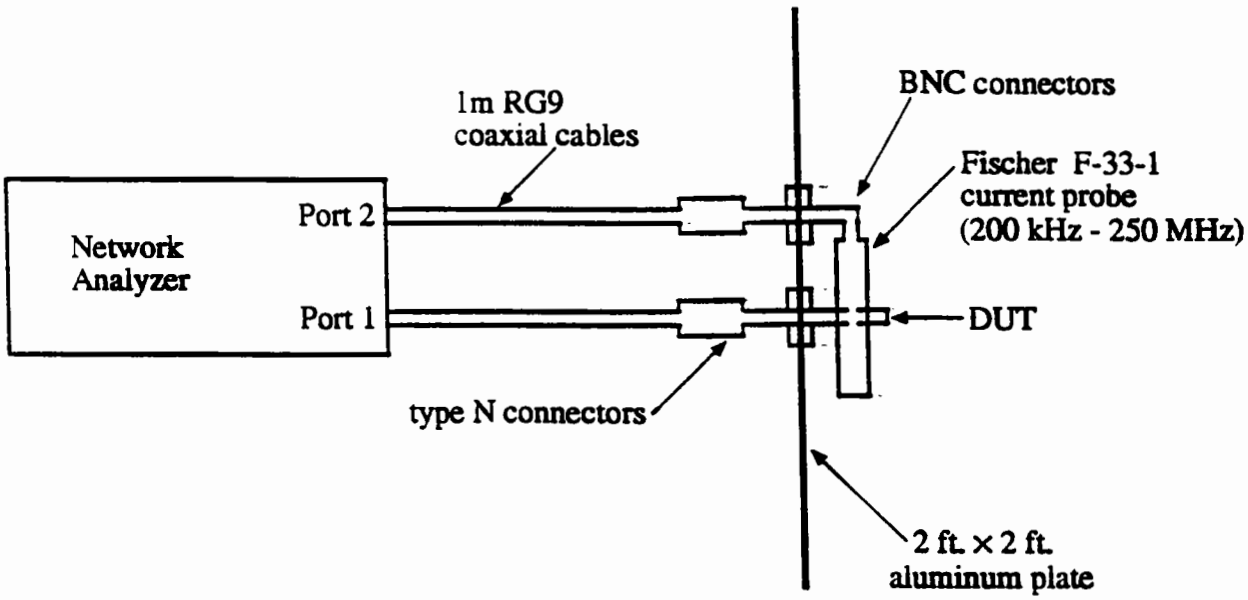

Figure 8: Experimental setup for investigation of circuit geometries with the HP8753C network analyzer.

network analyzer was employed for conducting experiments with passive wire circuit geometries. The experimental test layout is illustrated schematically in Figure 8. Port 1 of the network analyzer provided the source for the wire circuit, and the output of a common-mode current probe was input to Port 2. The source impedance for the device under test (DUT) was the 50 Ω impedance of the network analyzer, as opposed to the ideal source used above in the numerical examples. A $2' \times 2'$ square aluminum plate was used in all the measurement procedures in order to obtain a sufficiently large common-mode current to measure, and to provide a test environment from which repeatable measurements could be obtained. The measured common-mode current was not found to be a function of the network analyzer cable dressing when the aluminum plate was employed. The common-mode current was measured using a Fischer F-33-1 ($200\ kHz - 250\ MHz$) current probe. The error correction capabilities of the HP8753C network analyzer enabled the transfer impedance of the current probe to be included in the calibration procedures.

An experimental configuration that modeled the wire circuit geometry of Figure 3 (a) was constructed from coaxial cable as shown in Figure 9. The test device was measured with the network analyzer, and the results are shown in Figure 10. The common-mode current that results when $Z_L = \infty$ is due to the voltage driven mechanism, and is approximately 20 dB greater than for short circuit loading, corresponding to the current driven mechanism, for frequencies below the exhibited resonances. As discussed in the numerical examples, when $Z_L = \infty$, (i.e., the voltage

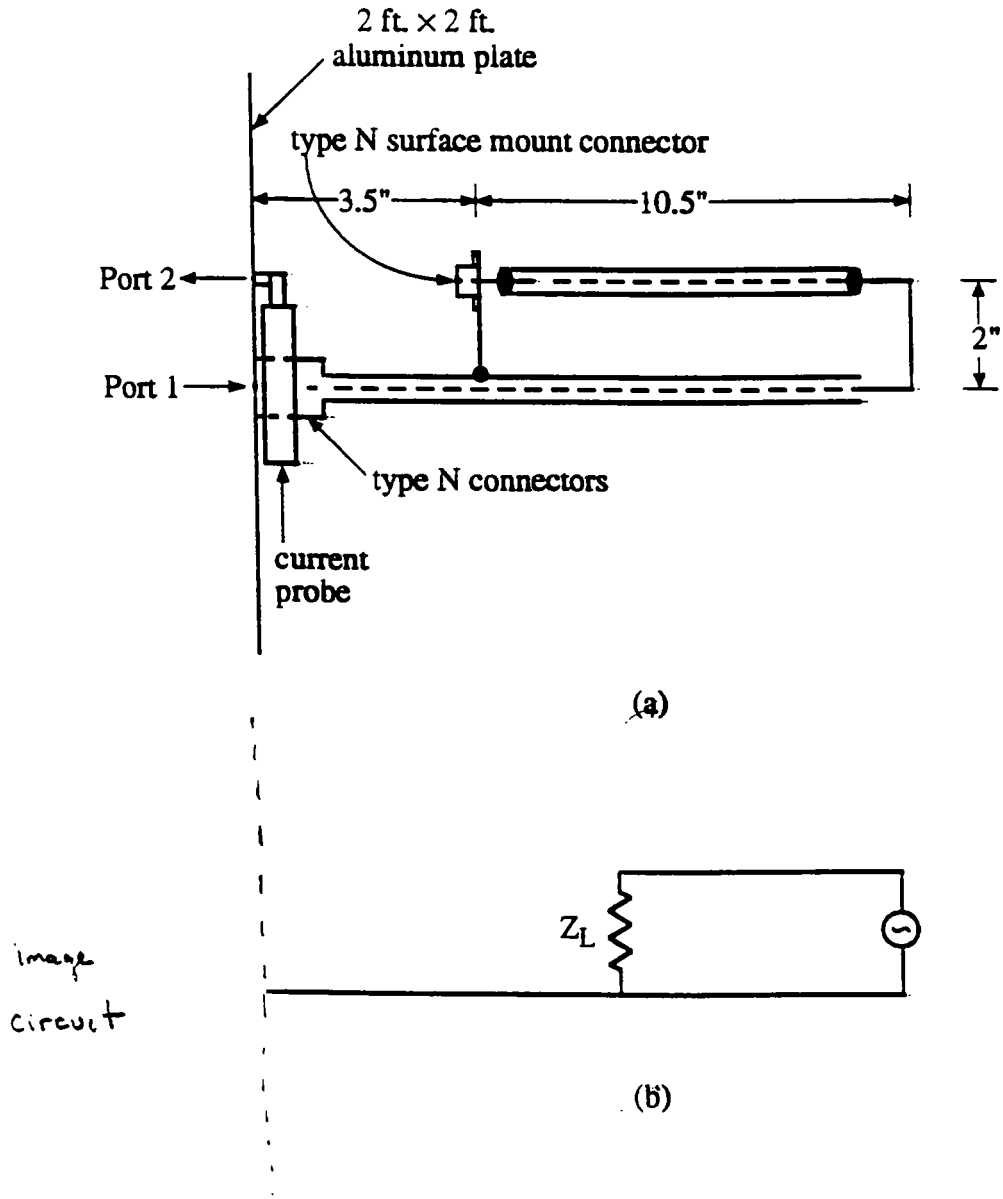

Figure 9: Coaxial cable test configuration. a) geometry, and b) equivalent wire circuit.

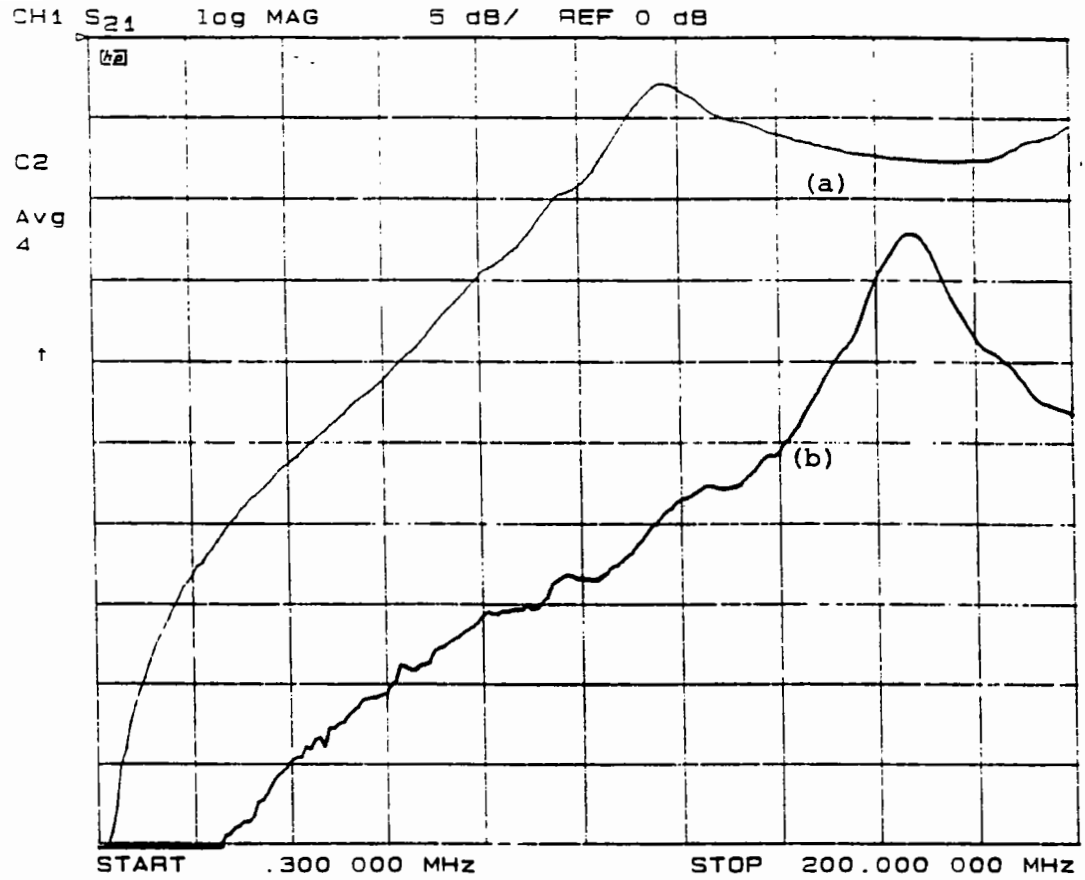

Figure 10: Measured results for the coaxial cable test configuration. a) Open and b) short circuit loading, corresponding to voltage and current driven mechanisms, respectively.

driven mechanism) the common-mode antenna has two halves of sufficient extent that can be driven effectively by the differential-mode source. Equivalently, the input impedance of the common-mode antenna is sufficiently small to result in significant common-mode current for the given driving source. For the case of the current driven mechanism, with $Z_L = 0$, a distributed common-mode voltage source is generated by the differential-mode current in the lower conductor of the loop. However, in this case, the common-mode antenna is being driven near one end, resulting in a very high input impedance, and little common-mode current is driven on the antenna. The resonance observed for $Z_L = \infty$ at 116 MHz is a quarter-wave monopole resonance. The wavelength at 116 MHz is 2.59 m, and a quarter wavelength is 0.65 m = 25.9″. The coaxial cable length above the small ground plane is 26.5″. The short circuit case is expected to produce a resonance at a higher frequency, since the effective length of the antenna is shorter. In this case there is 14″ of common-mode current path above the plate and the measured resonance occurs at approximately 167 MHz.

The current and voltage driven mechanisms were investigated for a smaller wire circuit more representative of printed circuit type geometries. The wire circuit geometry is shown in Figure 11. The Molex "jumper" connectors shown were employed to facilitate testing for open- and short-

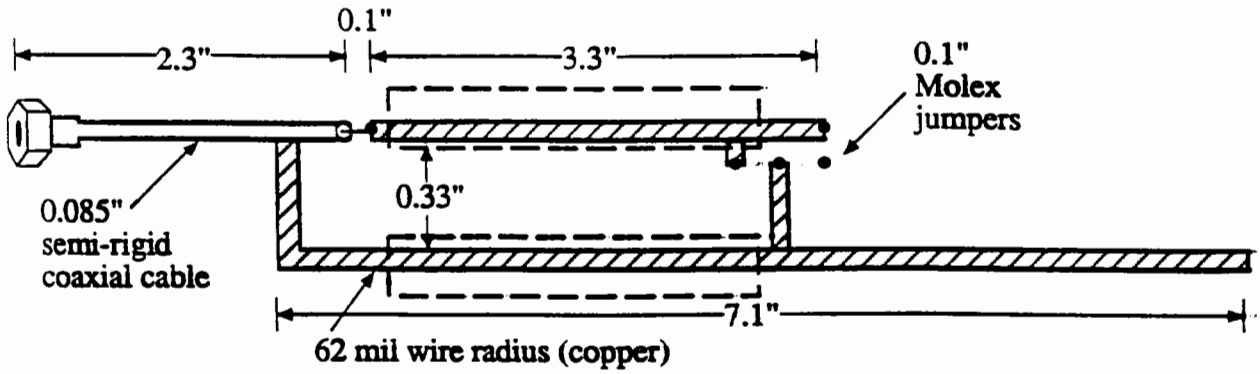

Figure 11: Wire circuit configuration for demonstrating the voltage and current driven mechanisms in printed circuit geometries.

circuit loading conditions. While the geometry is still large relative to typical printed circuit dimensions, the circuit demonstrates the fundamental physics under investigation. The circuit source was provided by the network analyzer, and the common-mode current measured as previously described. The results for both open and short circuit loading conditions are shown in Figure 12 (a). The measured data in curves (1) and (2) are for open circuit loading conditions. Curve (1) is the result for the circuit with the 3.3", 62 mil wire driven against the extended portion of the lower conductor (away from the ground plane), as well as against the semi-rigid coaxial cable and ground plane. In this case the resulting common-mode radiation might be expected to be small because the common-mode currents on the two extended portions of the lower conductor are in opposite directions. The data of curve (2) was obtained with an added 1 cm wide, 7 cm long strip of aluminum tape on the upper conductor as indicated by the dashed rectangle in Figure 11. The increase in conductor area has increased the capacitance between the driven upper conductor and the semi-rigid coaxial cable (and ground). The increased capacitance results in a decreased input impedance of the electrically short antenna, which results in an increased common-mode current as compared to the case of data (1).

The measured data for short circuit loading conditions are shown in Figure 12 (a), curves (3) and (4), as well as Figure 12 (b). The current in the short circuited loop is limited by the 50 Ω source impedance, as well as the loop inductance, which results in an impedance of approximately $j50\ \Omega$ at 100 MHz. The measured results indicate for this geometry, that the current driven mechanism is dominant for frequencies above 100 MHz. The data in curve (3) of Figure 12 (a) is for the 62 mil conductor wire loop. Strips of aluminum tape 1 cm wide and 7 cm long were added to the top and bottom segments of the differential-mode current loop as shown by the dashed rectangles in Figure 11 with the resulting common-mode current shown in curve (4) of Figure 12. The driving

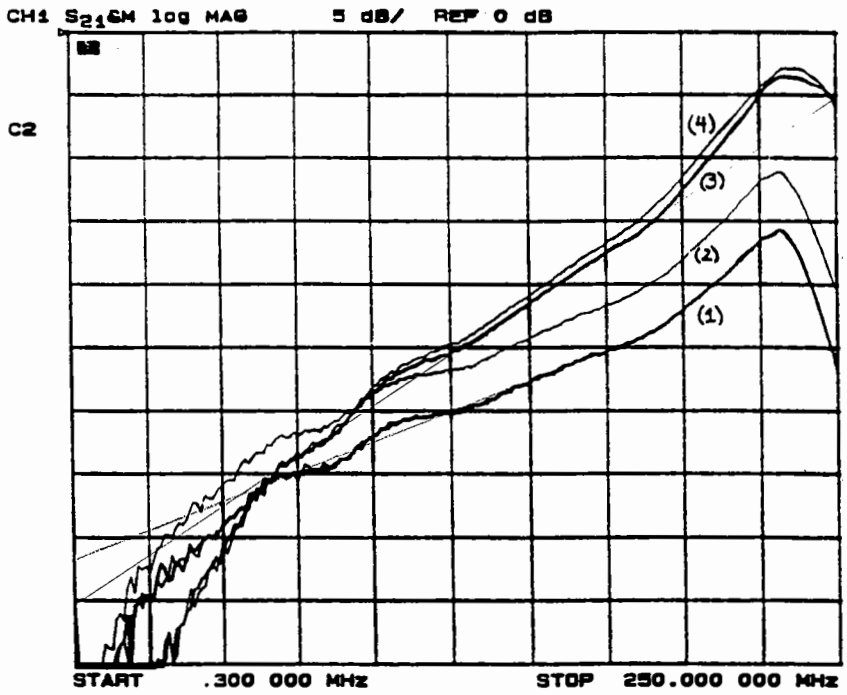

(a)

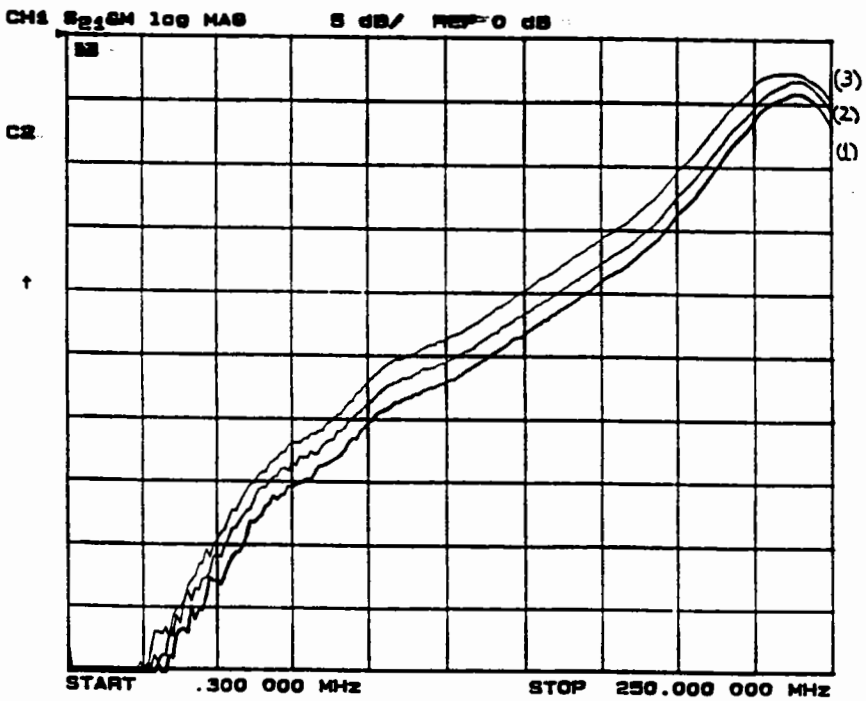

(b)

Figure 12: Results measured with the HP8753C network analyzer for the wire circuit geometry of Figure 11.

source for the common-mode current is the voltage drop produced by the differential-mode current through the lower segment of the differential-mode loop. The voltage drop results from the partial inductance of the lower conductor segment. The partial inductance of the lower or upper segments can be changed by adding a single aluminum tape strip to the segment as shown in Figure 11. The data for these cases are shown in Figure 12 (b). The data of curve (1) have the aluminum tape strip added to the bottom segment of the differential-mode loop, curve (2) is no strip added, and curve (3) is the strip added to the upper conductor. In cases (1) and (3) the differential-mode current is the same. The data illustrates what is expected for the current driven mechanism. When the aluminum strip is added to the upper conductor, more of the voltage dropped around the loop appears across the lower conductor as a result of lowering the partial inductance of the upper conductor. The voltage produced in the lower segment by the differential-mode current provides the driving source for the common-mode current on the antenna. Conversely, when the aluminum strip is added to the lower conductor, less of the total voltage is dropped along the lower segment. The driving source of the antenna is therefore reduced, and the resulting common-mode current is decreased, as observed from curve (1).

The resonance observed in each curve is a result of a quarter-wavelength resonance corresponding to the length of the lower conductor above the ground plane, in both the open and short circuit cases. The wavelength at 235 MHz is approximately 128 cm, and a quarter wavelength is 32 cm. The length of the lower conductor above the ground plane is approximately 29 cm.

The common-mode driving source for the current driven mechanism is $V_{CM} = j\omega\, M I_{DM}$. The partial mutual inductance M, can be decreased by increasing the width of the return conductor. This was investigated experimentally with a wire circuit geometry over a ground conductor as shown in Figure 13 (a). Measurements were obtained for a 1, 3, 5, 10, and 14 cm wide signal return conductor, and are shown in Figure 13 (b). The current is limited by the 50 Ω source impedance in series with the loop inductance. Using the approximate formula for a wire over an infinite ground plane, the loop impedance at 100 MHz was calculated to be approximately $j52\ \Omega$. It is observed that as the width of the signal return conductor is increased, the measured common-mode current decreases, which is consistent with a decreasing common-mode driving source.

The two fundamental mechanisms were investigated for a wide conductor configuration to simulate the DC power distribution bus in a single layer printed circuit geometry as shown in Figure 14 (a). The conductors were made large in order to obtain sufficient dynamic range for the measurements. The data for both open and short circuit loading conditions are shown in Figure 14 (b). In this case, the particular geometry chosen exhibits a resonance frequency sufficiently high

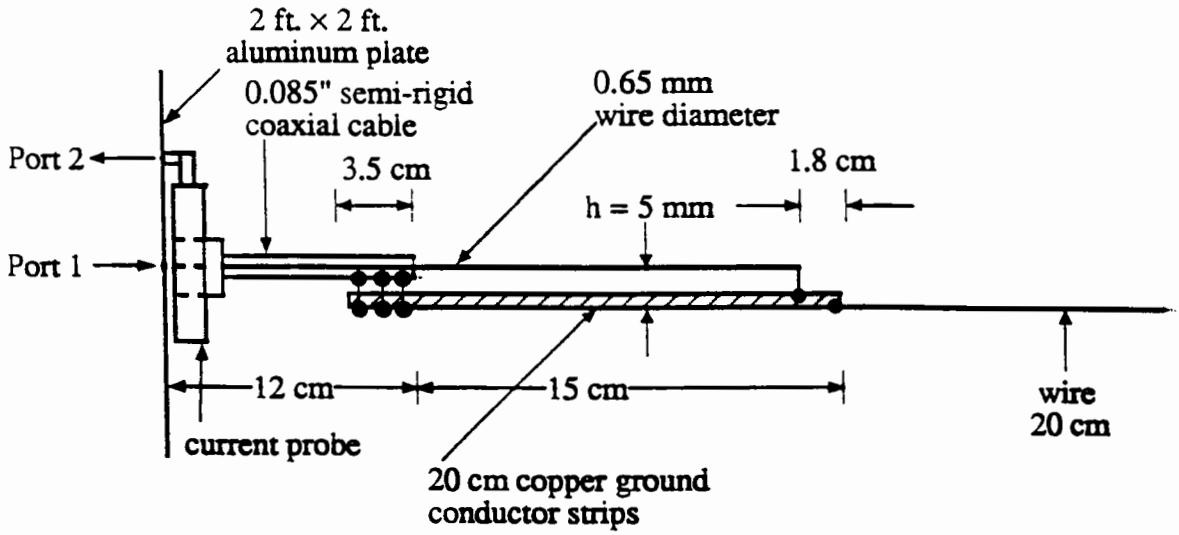

(a)

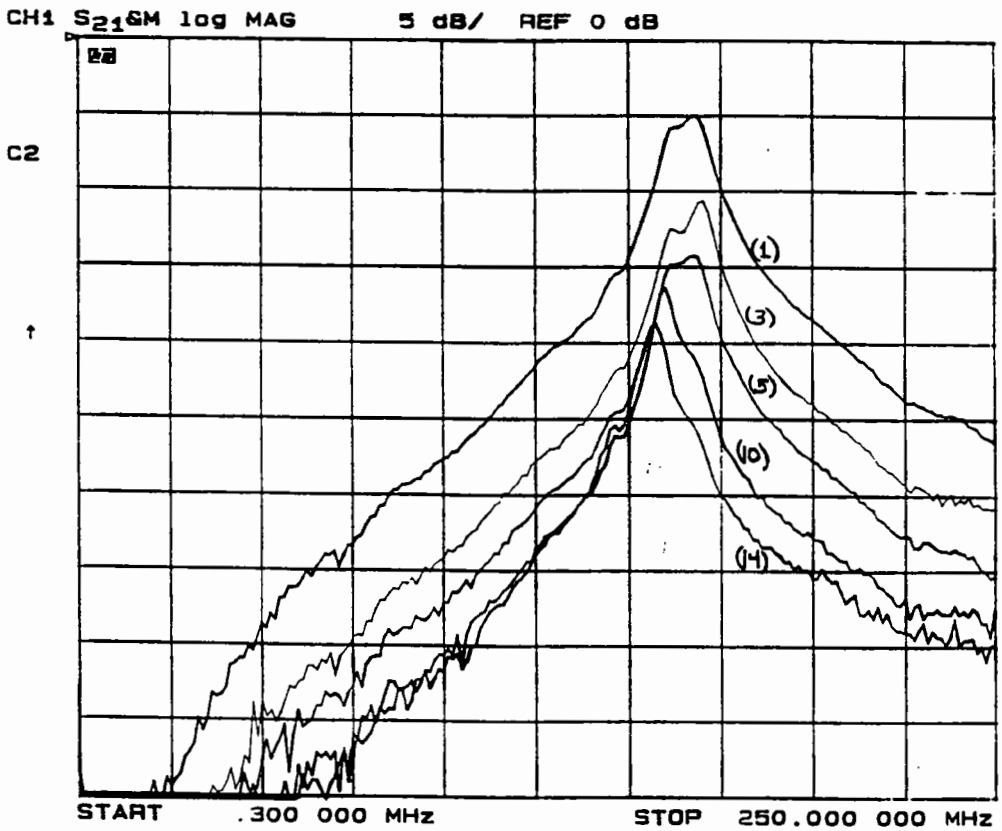

(b)

Figure 13: a) Circuit geometry for investigating the dependence of the current driven mechanism on the width of the signal return conductor. b) Data for signal return conductor widths of 1, 3, 5, 10, and 14 *cm*.

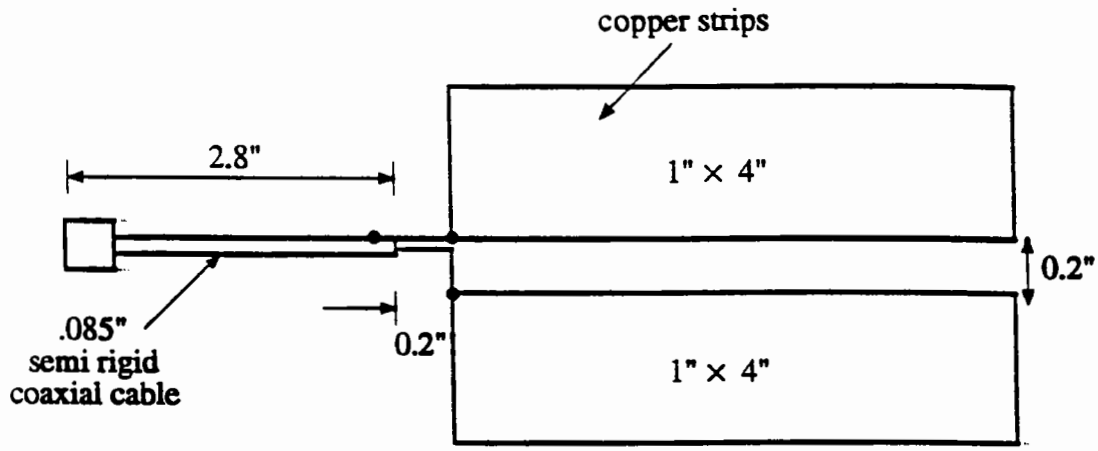

(a)

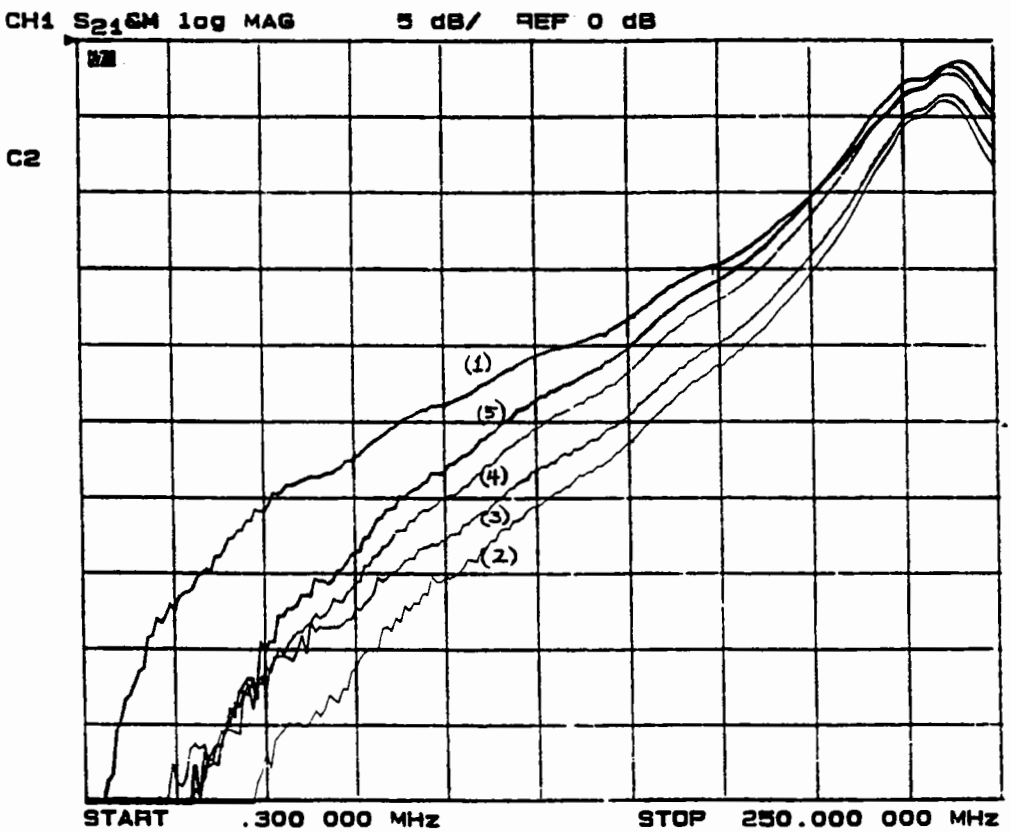

(b)

Figure 14: a) Circuit geometry for investigating the voltage and current driven mechanism on a configuration with significant metal area as might be the case for the DC power distribution bus. b) Results for an open circuit (1), and short circuit at 1" (2), 2" (3), 3" (4) and 4" (5) from the source.

that the low frequency behavior of the common-mode current is not obscured by the resonance. At frequencies below 150 MHz, the common-mode current produced by the voltage driven mechanism exhibits an increase with frequency of approximately 6 $\frac{dB}{octave}$. The measured common-mode current is related to the input impedance of the circuit and driving source by $I_{CM} = \frac{V_{DM}}{Z_{in}} \approx V_{DM}(\omega C)$, which is a 6 $\frac{dB}{octave}$ increase with frequency. For the current driven mechanism, a 4 mm wide strip of copper tape was used as a short in the driving loop. The current is again limited by the 50 Ω source impedance in series with the loop impedance due to the inductance of the conductors. The loop impedance is approximately in the range of $j10$ to $j60$ Ω at 100 MHz [12], for the four shorting locations. The shorting strip was placed at four locations 1", 2", 3", and 4" from the source. As expected, as the loop area increases, the common-mode driving source is increased, and the measured common-mode current increases. Measurements were also obtained for the return conductor extended an additional 4" in length, and the same behavior was observed. The low frequency behavior of the common-mode current for the current driven mechanism is given by $\mid I_{CM} \mid = \mid \frac{V_{CM}}{Z_{in}} \mid \approx \mid V_{CM} \mid (\omega C) = (\omega M)(\omega C)$, which is a 12 $\frac{dB}{octave}$ variation with frequency. The measured data for the current driven mechanism displays approximately this variation.

The resonance observed in the measured data near 235 MHz is associated with the length of the reference conductor above the ground plane. The length of the conductor above the ground plane is 21.8 cm. The wavelength at 235 MHz is 128 cm, and a quarter wavelength is 32 cm. The difference between the measured resonance frequency and that computed using a simple quarter-wavelength approximation is due to the width of the antenna conductor. The very wide antenna conductor serves to significantly decrease the resonance frequency [13].

3.2 Daytime Running Lamp Module

The principles detailed in the above sections were applied to reduce the common-mode radiation from a production printed circuit design supplied by General Motors. The circuit, denoted the Daytime Running Lamp (DRL) module, produced significant common-mode radiation in a frequency band around 50 MHz. Measurements of common-mode current were made using an HP8569B spectrum analyzer (10 MHz – 20 GHz). The output of the Fischer common-mode current probe was input directly to the spectrum analyzer. A schematic of the experimental setup is shown in Figure 15 (a). The DRL module was powered by a 12 V power supply. The power wires were 1 m long. A 1 m wire was also connected to the photocell input, and left unterminated to simulated the high impedance loading for daytime conditions. The common-mode current was measured 6" from the DRL with the Fischer F-33-1 current probe connected to the spectrum analyzer, and is

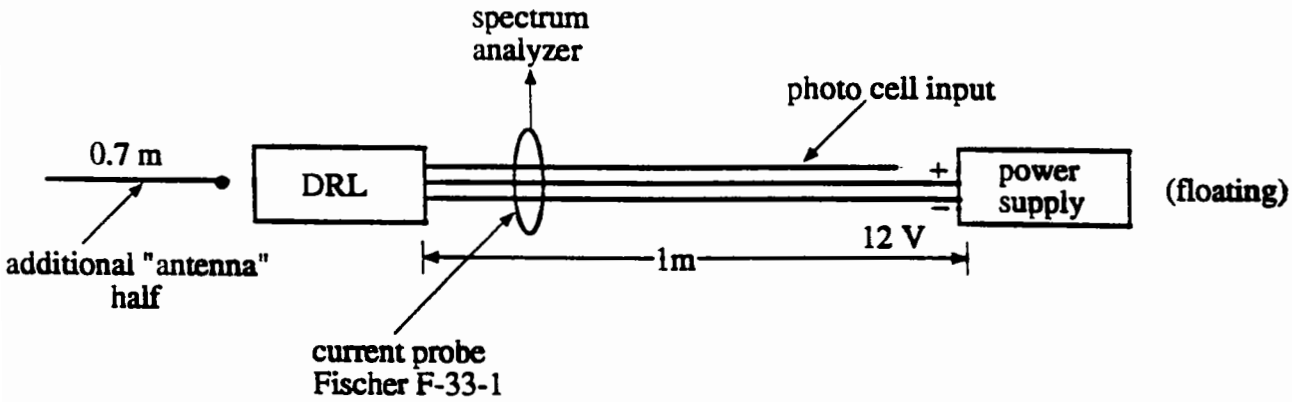

(a)

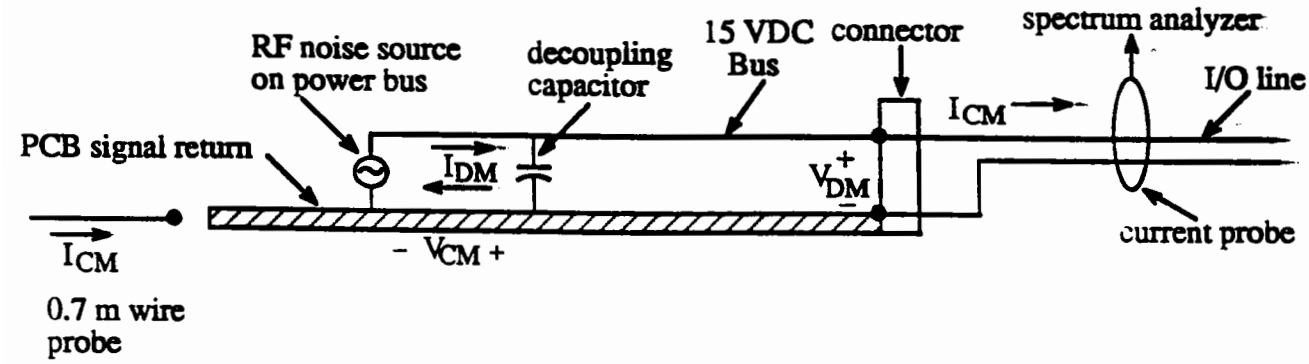

(b)

Figure 15: a) Experimental setup for common-mode current measurements on the leads to the DRL module. b) Reduced circuit model illustrating the fundamental mechanisms leading to common-mode radiation for the DRL module.

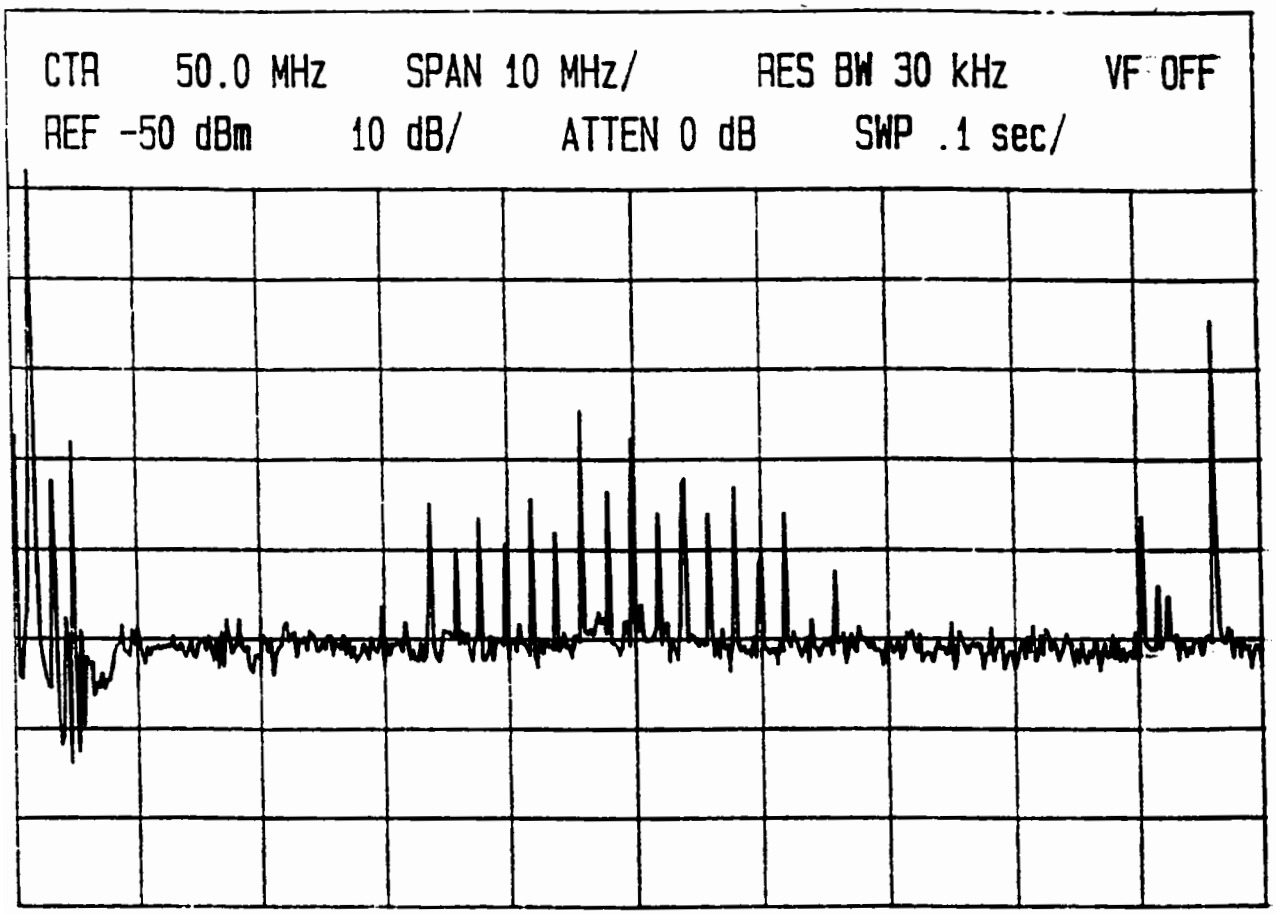

Figure 16: Common-mode current measured on the power and photocell input cable bundle.

shown in Figure 16. Significant common-mode current on the cable bundle is observed in a band around 50 MHz. The signal shown in the data below 10 MHz and for $90 - 100$ MHz is measured when the DRL module is unpowered, and is not associated with common-mode radiation from the DRL module. A simple 0.085″ semi-rigid coaxial cable probe with the center conductor extended was employed for measuring the RF voltage on the 5 V side of the DC power bus. Measurements were taken at several points between the power pins of the single on-board IC module and the photocell input pin at the connector (which is connected to V_{CC}). Significant noise over the entire 100 MHz band was measured, with a slight peaking around 50 MHz. A 100 nF decoupling capacitor was placed at the connector across the photocell input and ground. The common-mode current measured upon addition of the decoupling capacitor is shown in Figure 17. The addition of the decoupling capacitor decreased the measured common-mode current by at least 25 dB. The dynamic range of the measurements is only 25 dB (initial common-mode current above the noise floor), and it is possible that the common-mode current is decreased even further. Both surface-

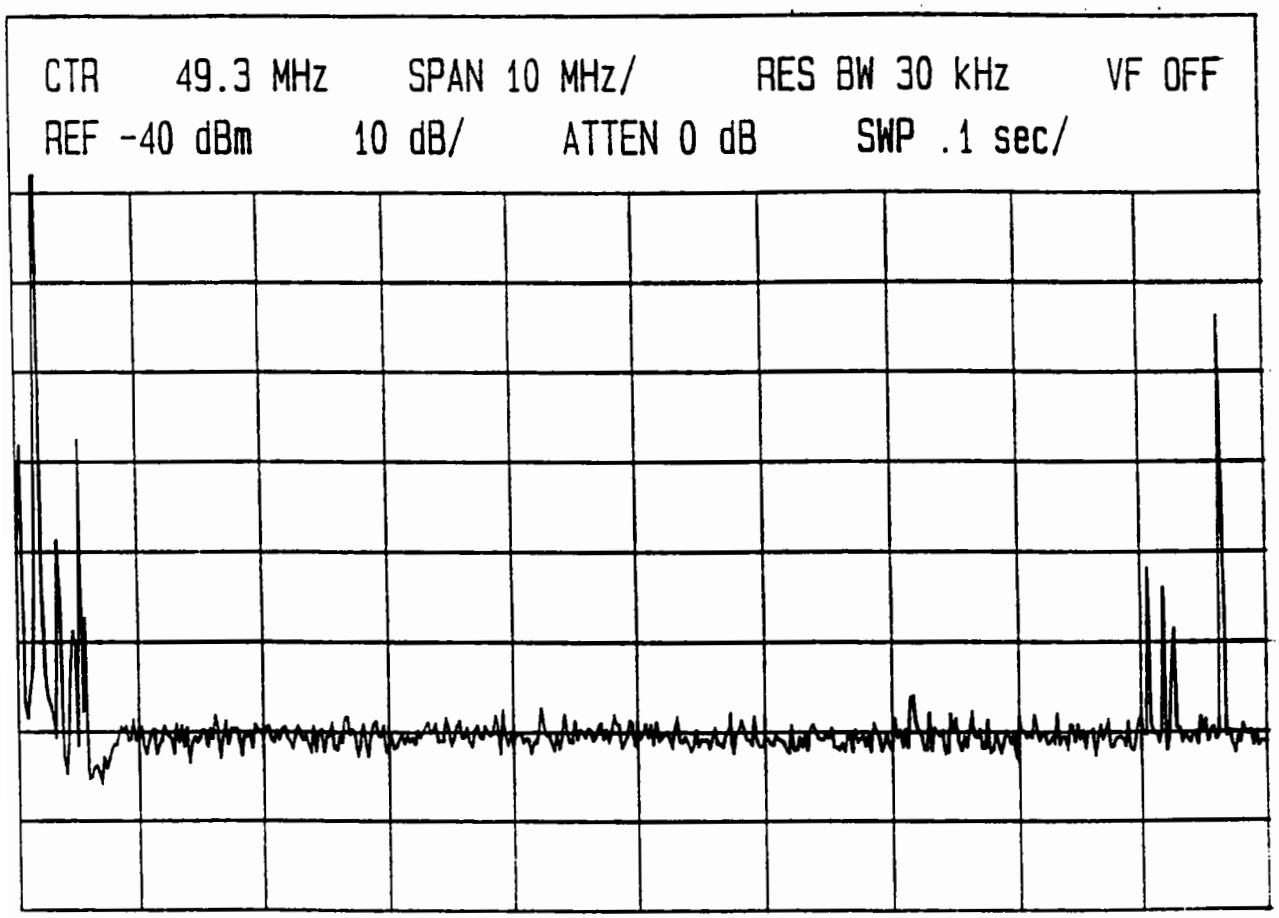

Figure 17: Common-mode current measured on the DRL power and photocell input cable bundle with a 100 nF decoupling capacitor across the photocell input pin and ground at the connector.

mount and leaded 100 nF capacitors were employed, and found to produce the same results within the dynamic range of the measurements. The leaded capacitor connecting wires were formed into an approximately square loop of dimensions 1.3 $cm \times 1.3$ cm. While the impedance of the leaded capacitor at 50 MHz will be of the order of several ohms, since the self resonance frequency is approximately 5 MHz, this is still small compared to the input impedance of the antenna that is driven by the differential-mode noise source. In the worst case, the common-mode antenna will be resonant, with a real input impedance of approximately 73 Ω. Thus even a leaded capacitor provides a lower impedance path than the radiator.

The dominant common-mode driving mechanism in this case is voltage driven. A simple model of the common-mode noise source and antenna on the DRL module is shown in Figure 15 (b). The driving source for the antenna is the differential-mode noise voltage on the 5 V power bus. This noise voltage, which is developed between the photocell input lead and ground as a result of the IC module switching (delta-I noise), is the differential-mode source that ultimately results in common-mode current on the photocell input and power lead cable bundle. The antenna is comprised of the photocell input lead and the extensive metal structures of several on-board relays that are directly connected to ground, as well as imbalances in the attached cable. The differential-mode noise voltage exists between these antenna halves, and provides a good driving source at the resonance of the antenna. The peculiar geometry of the common-mode antenna makes determining the antenna resonance frequency and input impedance very difficult. The wavelength at 50 MHz where the common-mode current exhibits a resonance is 6 m. For the source to be at the center of an equivalent half-wave dipole the length of the photocell input lead would have to be 1.5 m. The 1 m length of wire attached to the photocell input is somewhat shorter. However this length is in the range where the antenna input impedance might be expected to be of the order of a few hundred ohms, and thus be effectively driven by the differential-mode noise voltage source around the resonance frequency.

The measured common-mode current on the described cable bundle for the off-the-shelf configuration of the DRL module was found to be dominated by the voltage driven mechanism. However, as noted by Paul [14], the net effect observed in many EMC problems is often the sum of two or more components, one of which may be dominant for certain circuit configurations and/or frequencies. Upon further inspection of the reduced circuit model of Figure 15 (b), it is observed that the decoupling capacitor loop can provide a current driven mechanism type source, for driving a common-mode antenna. The large switching currents drawn by the IC module will produce a voltage drop on the ground conductor that can potentially drive two portions of the ground against

one another (as two halves of an antenna). The common-mode voltage source that results from the differential-mode switching current is further increased in the attempt to eliminate the voltage driven mechanism by placing a decoupling capacitor between V_{CC} and ground at the connector. The length of the differential-mode loop is increased, as is possibly the differential mode-current by the addition of the 100 nF capacitor at the connector. An increase in the loop inductance is expected, and hence an increase in the voltage dropped along the return conductor. The noise voltage at four points along the ground conductor was measured with the 0.85″ semi-rigid coaxial cable probe. A 100 nF decoupling capacitor was connected between the photocell input and ground at the connector. The measured RF voltage at the connector, a point midway between the connector and the location of the IC module decoupling capacitor, at the IC decoupling capacitor, and at the ground pin of the IC is shown in Figure 18. It is observed that there is a considerable difference in the RF noise voltage over the extent of the differential-mode switching current loop. This variation in the voltage is consistent with what is expected with the current driven mechanism.

The decoupling capacitor loop, and the loop with the added 100 nF provides a common-mode voltage source that can drive an antenna. However, the judicious placement of the IC module in the far corner of the printed circuit board has effectively placed the common-mode voltage source very close to the end of the potential antenna. The high input impedance seen by the driving voltage source then results in unmeasurable common-mode current. A lower input impedance antenna can be artificially provided by connecting a wire to the ground conductor on the side of the IC package opposite the connector. This places the common-mode voltage source produced by the differential-mode current, approximately in the middle of the antenna, thereby lowering the input impedance. The common-mode current measured on the photocell input and power lead bundle for this configuration is shown in Figure 19. Common-mode current on the cable bundle is observed in frequency bands around 40 and 60 MHz.

4 Diagnosing and Reducing Common-Mode Radiation from Printed Circuit Designs

The first objective of this project was to investigate fundamental mechanisms by which differential-mode voltages and currents produce common-mode currents on radiating structures, which in turn produce undesired common-mode radiation. Once these mechanisms are known, systematic test procedures can be developed to determine which mechanisms dominate in a specific design. Two mechanisms have been identified that produce RF noise sources, which, if effectively connected

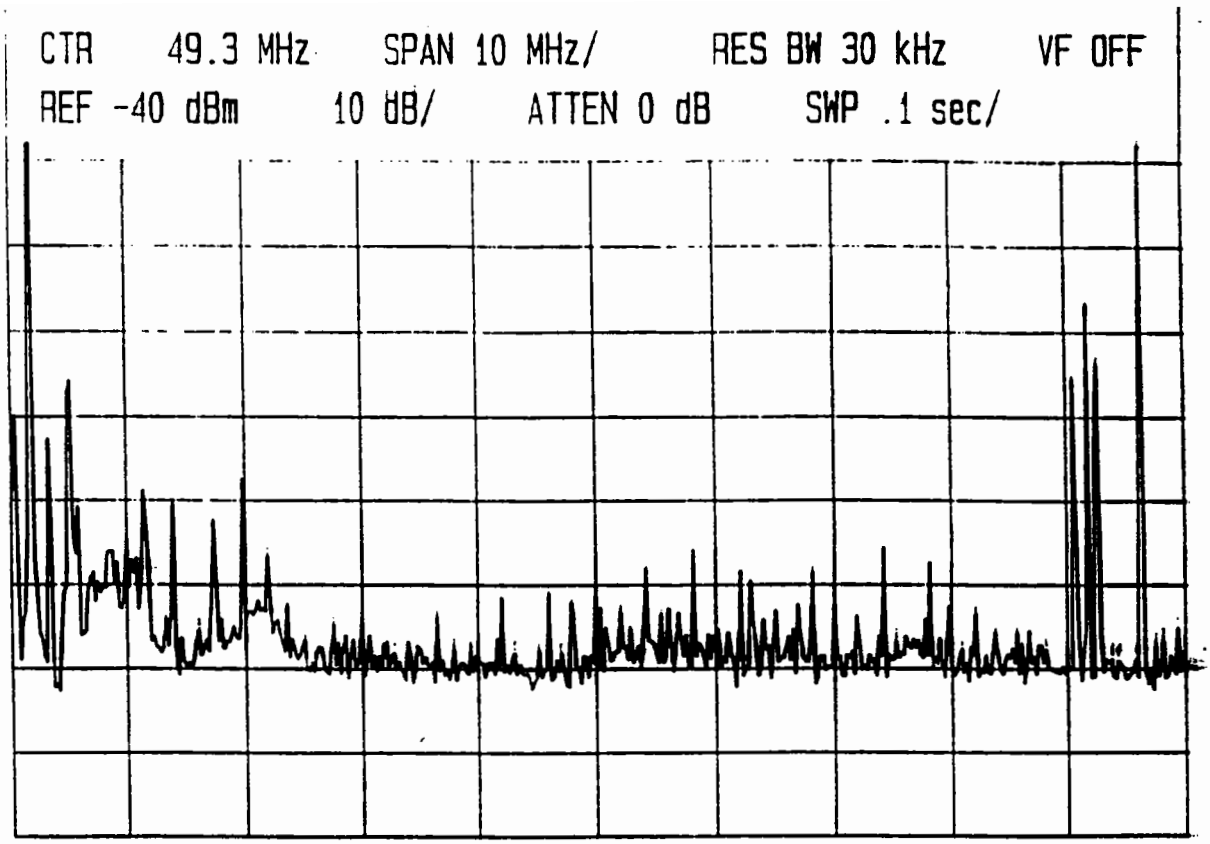

(a)

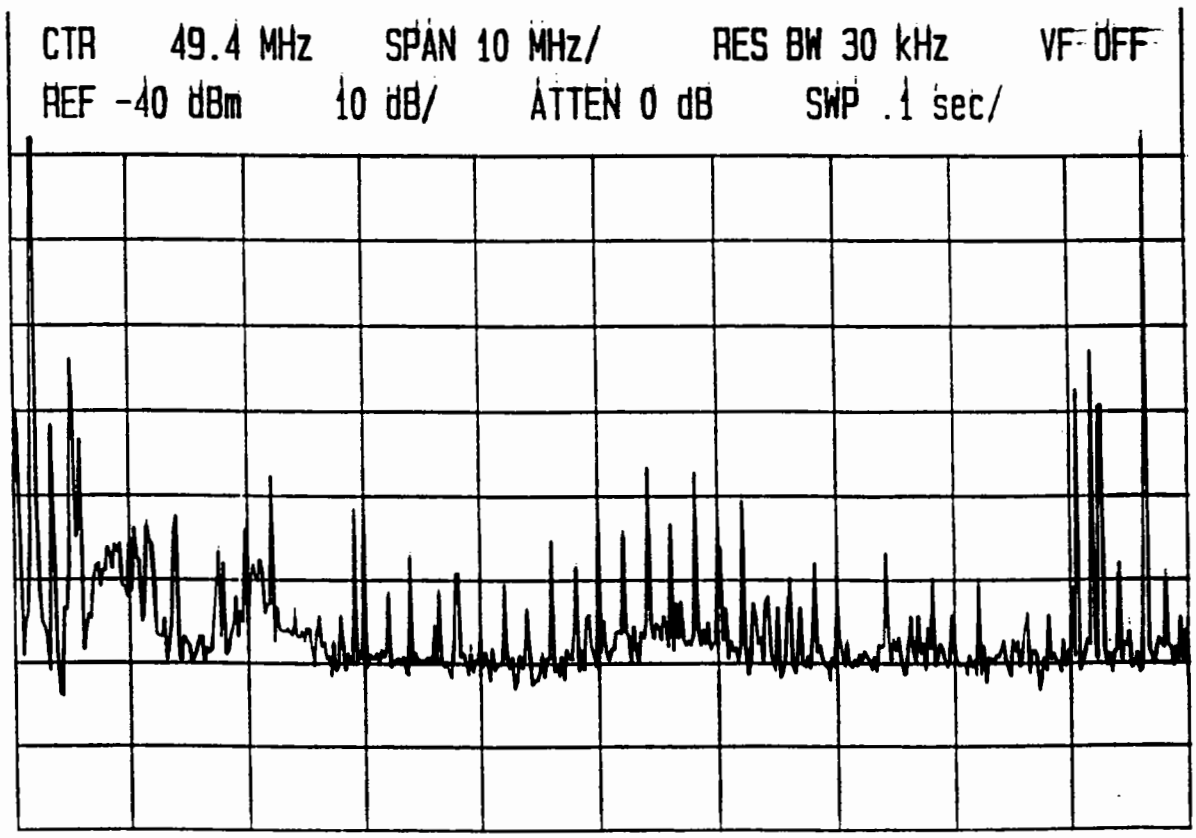

(b)

Figure 18: RF noise voltage on the ground conductor with a 100 nF capacitor placed at the connector. a) at the connector b) midway between the connector and location of the IC module decoupling capacitor

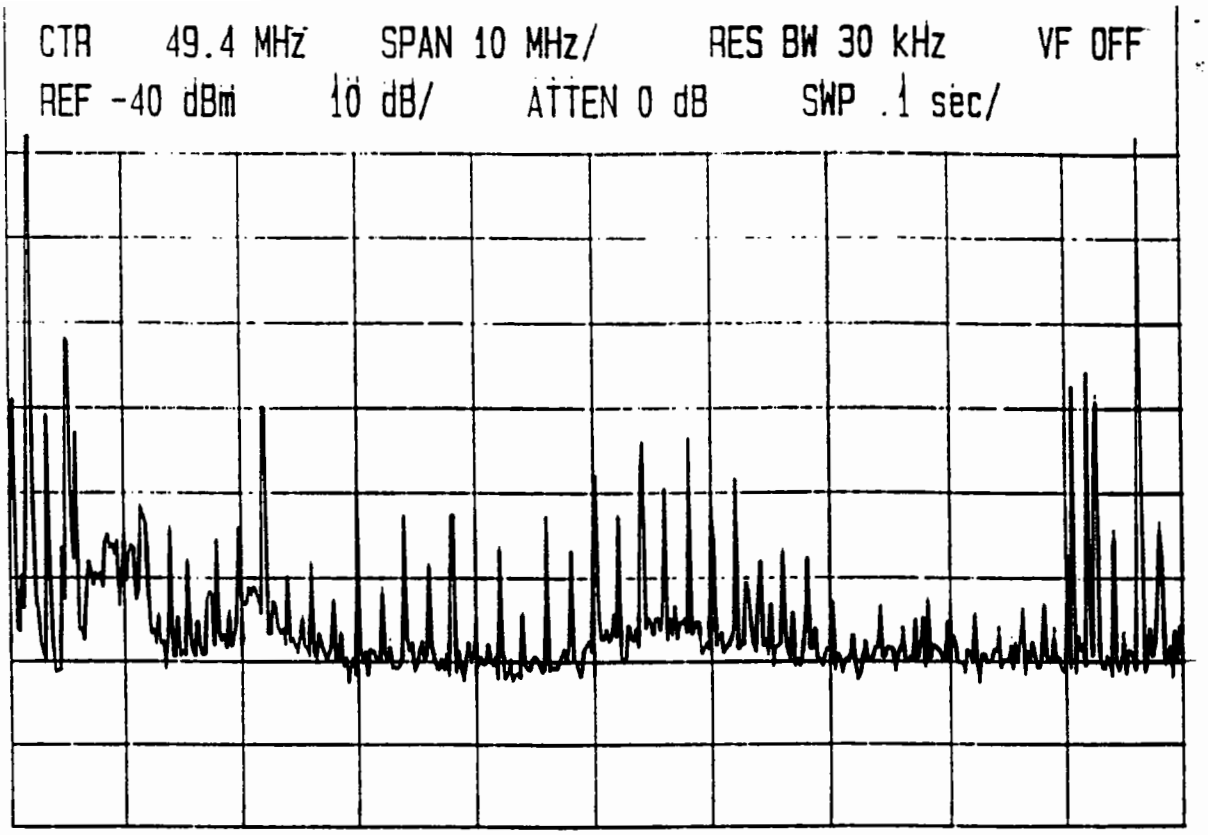

(a)

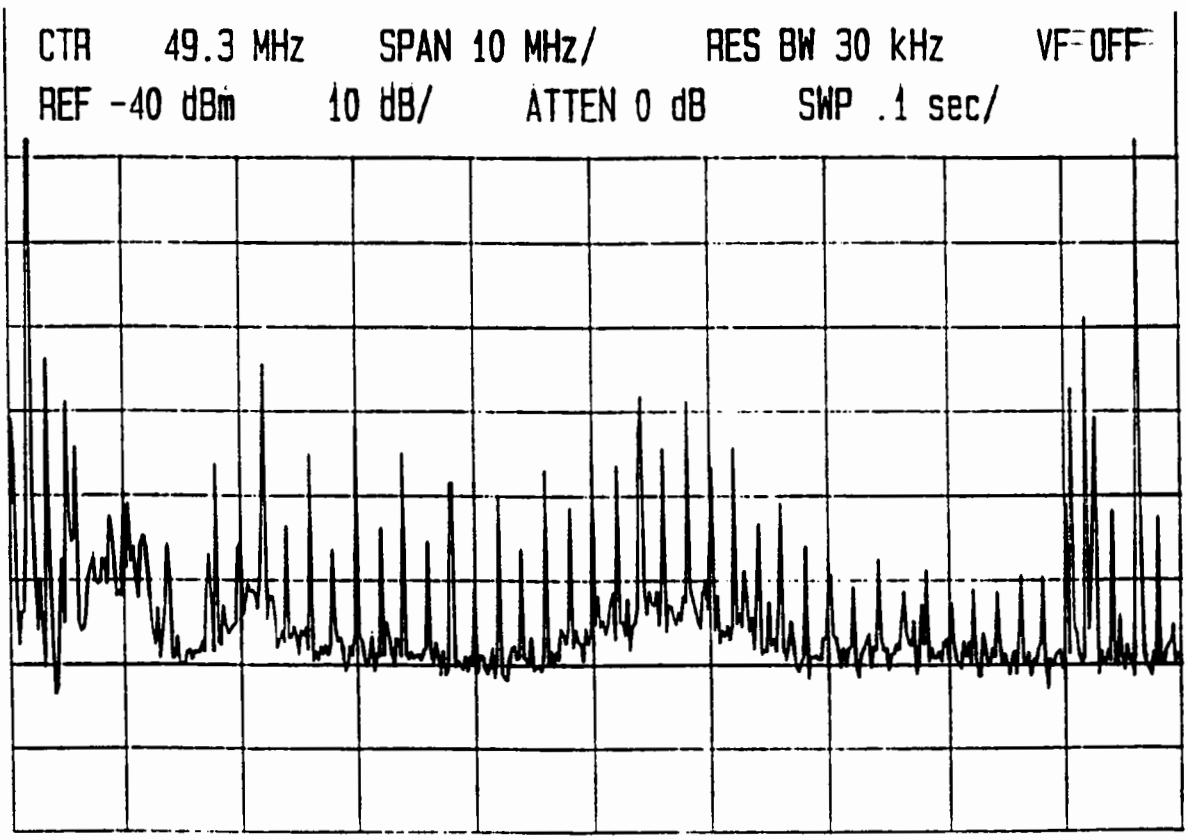

(b)

Figure 18: RF noise voltage on the ground conductor with a 100 nF capacitor placed at the connector. c) at the IC decoupling capacitor, and d) at the ground pin of the IC.

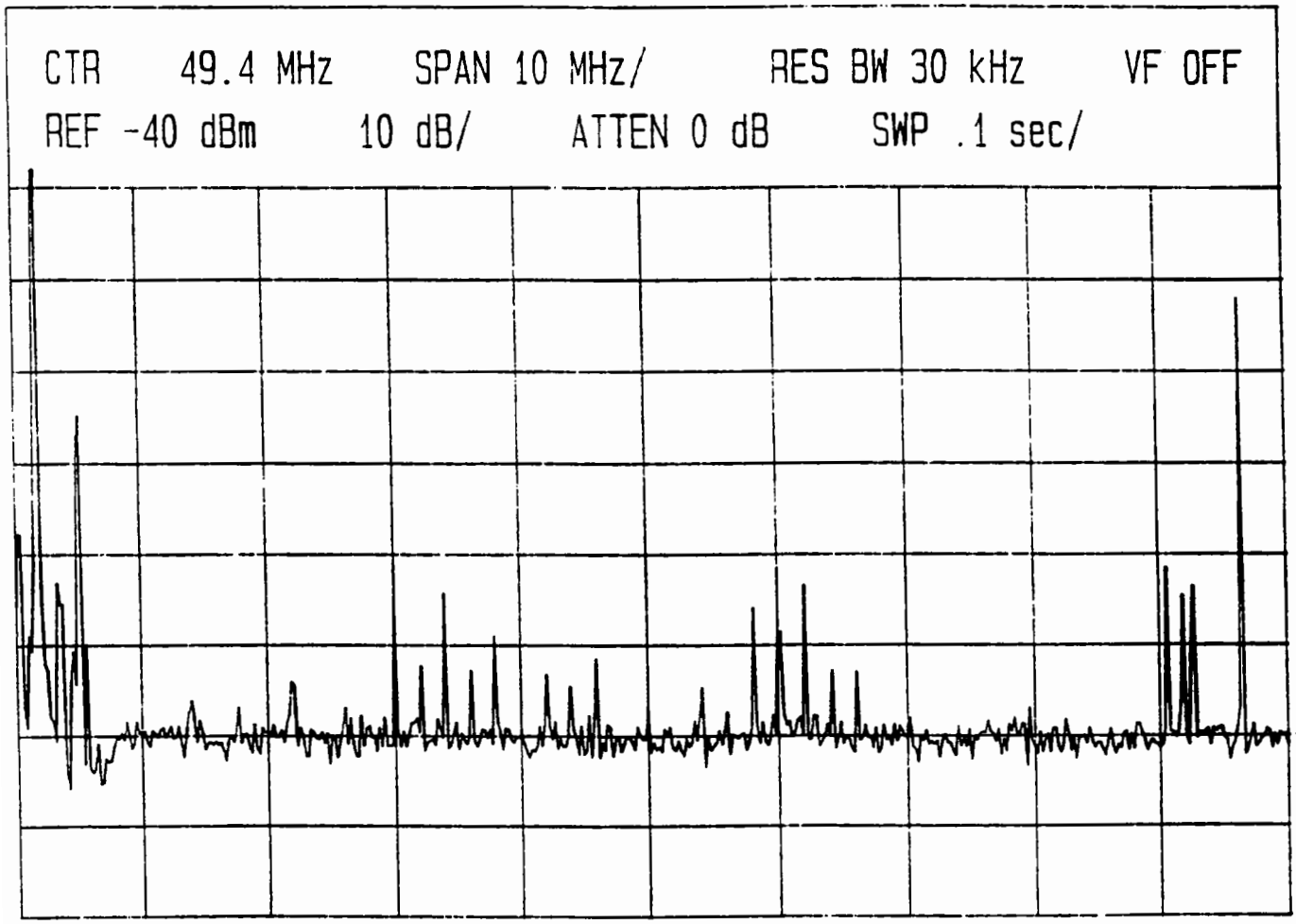

Figure 19: Common-mode current measured on the photocell input and power lead cable bundle with a 0.7 m wire attached to the ground conductor on the side of the IC package opposite the connector.

to an antenna can result in common-mode radiation. The second objective was to provide EMC engineers and circuit designers with strategies and techniques, based on the source mechanisms and a knowledge of common-mode antenna geometries, for determining or avoiding circuit configurations that result in common-mode radiation in printed circuit designs.

4.1 Basic Source-"Antenna" Configurations

Common-mode radiation requires both an RF noise source and effective connection (sufficiently low input impedance) of the source to an antenna. Figure 20 illustrates five basic RF source and antenna configurations that might lead to common-mode radiation. Typically, the conductor(s) in the attached cable bundle (I/O lines and signal return) will comprise at least one half of the antenna. The source driving the antenna is often much more difficult to discern than the antenna. A significant example of an antenna driving source that results from the voltage driven mechanism is the differential-mode noise voltage on the DC power distribution bus (delta-I noise). An example of an RF noise source resulting from a differential-mode current is the switching current in a decoupling capacitor loop. These examples are certainly among the more obvious sources, however, V_{DM} and I_{DM} in Figure 20 represent any high frequency differential mode voltage or current on the printed circuit board.

The five cases are ranked approximately in the order of severity of the resulting common-mode radiation problem. The configuration shown in (1) is a voltage driven mechanism and will result in significant common-mode radiation. The differential-mode RF noise voltage in many cases can be of significant amplitude, for example, the noise voltage on the DC power bus. This is essentially the configuration that resulted in common-mode radiation from the DRL module. A noise voltage on an I/O conductor will usually cause a common-mode radiation problem, because there is typically sufficient ground structure or metal directly or indirectly connected to ground on the printed circuit board to provide the other half of the antenna. If the metal structure is of sufficient extent, the input impedance seen by the source will be sufficiently low to result in appreciable common-mode current. In addition, sufficient imbalances in the I/O cable and/or load can provide an effective equivalent antenna in the cable bundle. Since the DC power bus is a known source of high-frequency noise, all I/O lines connected to V_{CC} should be decoupled at the connector. Likewise, all I/O lines connected to known RF noise sources on the board should be decoupled at the connector.

The configuration in (2) is a current driven mechanism, however, magnetic coupling to a secondary loop results in a differential-mode voltage source driving an antenna of the same type shown

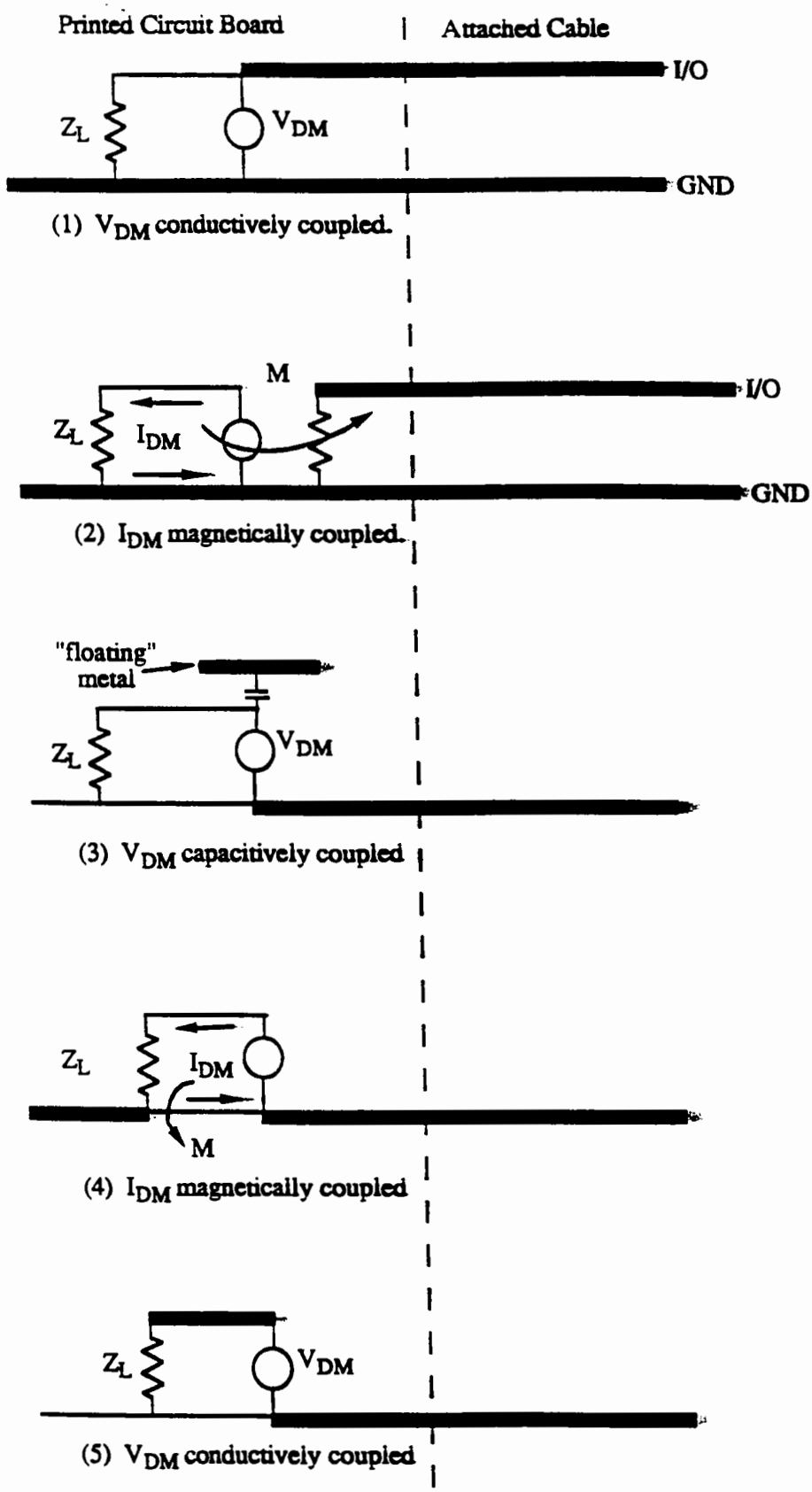

Figure 20: Five basic RF source and antenna configurations that might exist in a printed circuit design. V_{DM} and I_{DM} represent any high frequency differential-mode voltage or current, respectively, on the printed circuit board. The potential antenna conductors are indicated by bold lines.

in (1). Although the magnitude of the resulting differential-mode voltage at the connector may be of smaller amplitude than in the conductively coupled case of (1), magnetically coupled noise sources are usually much more insidious and difficult to determine. Cases (1) and (2) are likely to dominate common-mode radiation problems if unfiltered I/O lines are used. Even if shunt capacitive filtering is used on all I/O lines, common-mode radiation of the type illustrated in cases (1) and (2) may still be troublesome because of excessive inductance in series with the shunt capacitance. At higher frequencies excessive series inductance will render the capacitance even less effective. It is difficult to distinguish between cases (1) and (2), since in both instances a differential-mode voltage is produced between an I/O line and ground (signal return).

The equivalent common-mode antenna in (1) and (2) can be of two types. In one case the antenna may be entirely the cable bundle, where the common-mode current results from imbalances in the cable itself, and/or the load to which the I/O line is attached. In the other case, the antenna might be comprised of two distinct halves, one being the driven I/O cable, and the other half being the ground structure on the printed circuit board, and any extended ground to which it might be directly or capacitively coupled.

The voltage driven mechanism in (3) is similar to the configuration shown in (1), however, in this case the signal return conductor is the antenna half in the cable bundle, and the driven conductor is a large floating metal structure that is capacitively coupled to the noise source. The resulting antenna can have a low input impedance, and, if the coupling path is of sufficiently low impedance, significant common-mode current can result on the cable bundle (and floating metal structure). The configuration shown in (4) is current driven, and similar to (2), can present significant problems in determining the source, as well as the other half of the antenna. If the differential-mode current loop is positioned on the printed circuit board in a location that results in a low antenna input impedance, common-mode current will be driven on the attached cable bundle. However, if a high differential-mode current loop is known to exist, and the printed circuit judiciously layed out, the current loop and resulting common-mode source might be placed effectively at one end of the antenna, as is the case for the DRL module.

Determining the source mechanism, voltage or current driven, as well as the entire antenna structure is important in order to pursue a successful strategy for minimizing or eliminating common-mode radiation. Upon inspection of Figure 20, it is clear that certain measures which might prove beneficial in eliminating common-mode radiation from one type of source configuration, may have no significant effect, or may worsen the radiation produced by another type of source. The effect of circuit geometry and layout on the common-mode current on an attached

cable bundle for the noise sources shown in Figure 20, is given in Figure 21. Several different configurations relating to design choices and I/O decoupling are given.

4.2 A Diagnostic Procedure

A diagnostic procedure for determining which of the previously described five scenarios is the primary contributor to common-mode current on a cable attached to a printed circuit board is outlined in Figure 22. Cases (1) and (2) are expected to dominate common-mode radiation problems in the $10-200\ MHz$ frequency range if the majority of the printed circuit board inputs and outputs are not filtered. A detailed diagnostic procedure is described that is to be conducted without a ground plane beneath the printed circuit board and cable.

STEP 1: Begin with the printed circuit board or device under test (DUT) having the minimum number of wires connected to operate the digital clock. Ideally this will consist of the +VDC and ground (return) only. Measure the RF common-mode current on this group of wires using a clamp-on current probe. If the CM current is acceptably small, proceed to STEP 3. If the measured common-mode current is appreciable (based on past experience), proceed to STEP 2.

STEP 2: Provide temporary capacitive shunt decoupling at the connector between each wire in the bundle and ground. If the common-mode current is unaffected, then cases (3), (4), or (5) are present. Further investigation is required as detailed in STEP 4, upon completion of STEP 3.

STEP 3: Measure the RF output voltage from each connector lead as shown in Figure 23. A simple coaxial-cable probe (for example 0.85" semi-rigid) with an extended center conductor is sufficient for the measurement. The cable can be grounded at the spectrum analyzer, but the outer conductor (shield) should not be connected to the device under test. By placing the coaxial cable parallel to the device cable, sufficient capacitance to ground results to yield reliable and repeatable measurements. The lack of a ground lead greatly simplifies the measurement procedure. Determine the connector leads that are significant RF noise sources as illustrated in Figure 23. These leads are likely to result in common-mode current on the cable bundle as indicated in (1) and (2) in Figure 20. During this test, it is imperative that no wires in the cable bundle be connected to pins on which an RF voltage exists. If any cable wire is energized, then the remaining connector pins may produce a measurable RF output as a result of the probe capacitively coupling to the one energized wire.

STEP 4: Monitor the common-mode current on the $+12\ VDC$ and ground wire pair while probing

Priority rating in terms of ability to cause cable CM current.	1	2	3	4	5
Basic RF source configurations that might exist on a PCB.	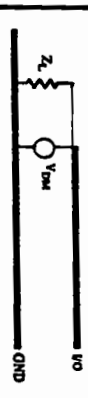		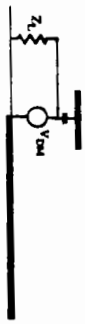		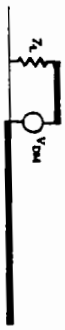
Add a capacitor between I/O line and ground at the connector with I/O and ground wires connected.	←	←	×	×	×
Connect only a ground wire.	×	×	→	→	→
Connect only an I/O wire.	→	→	→	→	→
Add an I/O wire with the ground wire already in place.	→	→	×	×	×
Add a ground wire with the I/O wire already in place.	←	←	×	×	×
Place a shield around the cable I/O and ground wires and connect shield to PCB ground at connector.	←	←	×	×	×
Connect any floating metal (e.g. heat sink) to PCB ground at connector.	×	←	←	→	←
Connect any floating metal to PCB ground opposite the connector.	→	→	→	→	←
Widen the PCB ground plane.	×	×	×	←	×
Unnecessarily extend the PCB ground plane area on the side opposite the connector.	→	→	×	→	×
Increase the impedance of the high frequency noise loop.	→	←	→	←	→
Place all connectors on a single side of the PCB.	←	←	×	←	×
Connect PCB ground to the metal enclosure at the connector	→	→	←	←	←
Grounding PCB opposite the connector.	→	→	×	→	×
Minimize the length of high I_{DM} loop.		←		←	
Locate HF circuits away from connectors.	×	←	×	←	×

Techniques That Might Change the Cable CM Current

Figure 21: Change in the common-mode current on attached cables as a result of changing circuit board or cable configuration for the five basic noise source equivalent circuits. ↑ indicates an increase in the common-mode current on the attached cables, ↓ indicates a decrease, × indicates no significant change.

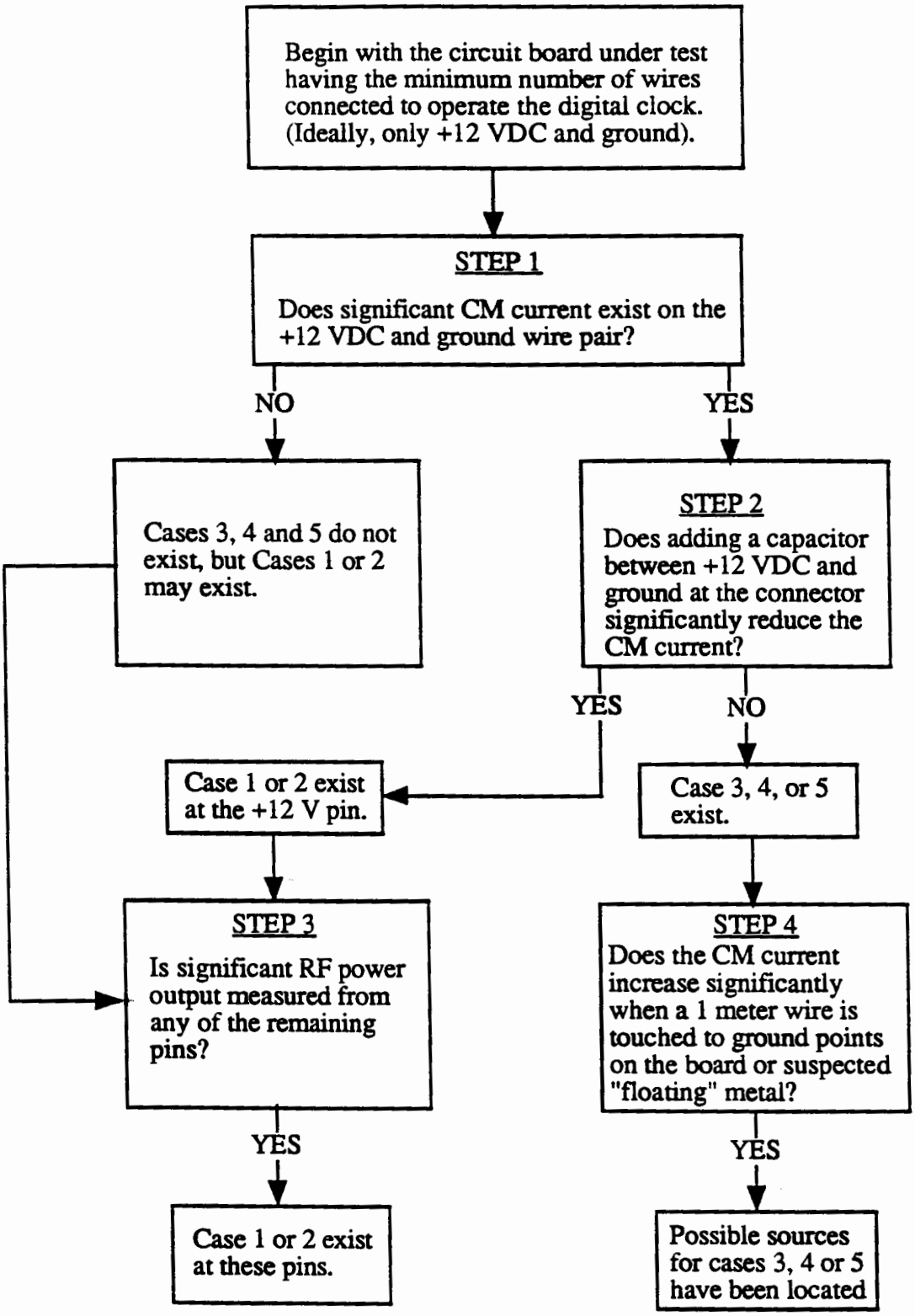

Figure 22: Flowchart outlining the diagnostic procedure for determining which of the cases shown in Figure 20 is the source of common-mode current on the cable bundle.

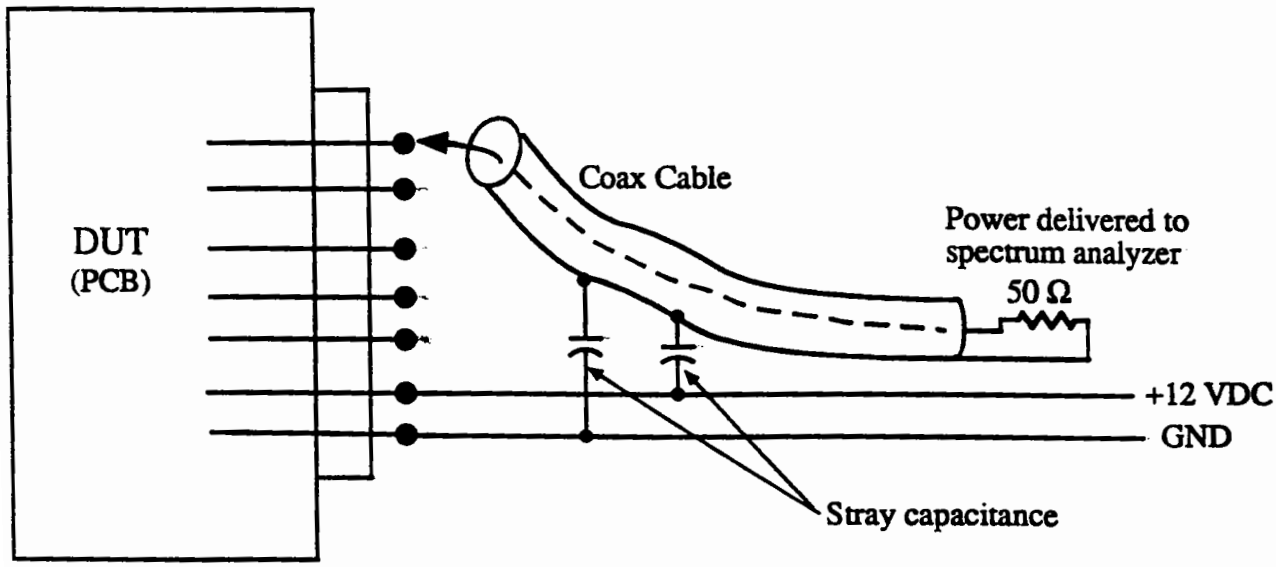

Figure 23: Test configuration for measuring the RF output at each connector pin.

various points of the circuit with a 1 m (approximate length) wire. The objective is to determine the location of sources on the printed circuit board that can drive "common-mode antennas", one-half of which is the attached cable ground wire as indicated in (3)-(5) of Figure 20. The long-wire probe then serves as the other half of the antenna. Various points on the ground structure should be probed as well as any floating (ungrounded) metal. The larger the metal surface, the greater the potential for producing significant common-mode current on the cable bundle. All ungrounded heat sinks should be investigated. The results of this test will become more informative as experience is gained in probing the printed circuit board and relating the observed effect on the measured common-mode current to the sources indicated in (3)-(5). In many cases, probing the printed circuit board will result in increased measured common-mode current because the second half of the antenna has been artificially provided. In the actual operating environment of the circuit, the driving source may not be as effectively connected to a second antenna half as can be provided by direct probing with a 1 m wire. However, through a knowledge of potential source locations, direct or capacitive coupling to a voltage or current driven noise source can more easily be determined.

5 Summary

The fundamental mechanisms leading to common-mode radiation from printed circuit designs have been investigated. Most often, the antennas involved in common-mode radiation are of the wire-type, i.e., comprised of two-halves driven by a potential difference. An attached cable bundle typically provides one-half of the antenna. Two mechanisms by which differential-mode voltages and currents result in common-mode current on a radiating structure have been identified. These two mechanisms have been denoted the voltage and current driven mechanisms. Minimizing common-mode radiation then corresponds to eliminating the driving source, or configuring the circuit geometry such that the antenna which can be driven by a source is ineffective. The two source mechanisms were identified and studied through numerical and experimental studies. The fundamental principles obtained from these studies were applied to a production circuit, the DRL module, provided by General Motors. The source mechanisms and antennas were identified based on insight gained from the investigation of the fundamental physics, and a means for minimizing the common-mode radiation was determined. A knowledge of the fundamental types of sources, and the antennas that these sources can drive, will provide EMC engineers with techniques and strategies for determining and reducing common-mode radiation problems in printed circuit designs. Five equivalent source and antenna geometries that might arise in a typical printed circuit design were provided, based on the two fundamental source mechanisms identified, to assist an EMC engineer in characterizing and reducing a common-mode radiation problem. A partial matrix of design options that might be available to circuit designers was constructed to assist in determining the effects of design choices on common-mode radiation from attached cables for the five equivalent circuits provided. Finally, a diagnostic procedure was given to provide a sytematic approach for determining the type and location of common-mode sources in a printed circuit design.

References

[1] C. R. Paul, *Introduction to Electromagnetic Compatibility*, Wiley-Interscience, New York, 1992.

[2] W. Stutzman and G. A. Theile, *Antenna Theory and Design*, John-Wiley, New York, 1981.

[3] C. R. Paul and D. R. Bush, "Radiated Emissions from Common-Mode Currents," *IEEE Electromagnetic Compatibility Symposium Digest*, September 1987.

[4] C. R. Paul, "A comparison of the contributions of comm-mode and differential-mode currents in radiated emissions," *IEEE Trans. Electromagn. Compat.*, vol. 31, pp. 189-193, May 1989.

[5] T. H. Hubing and J. F. Kauffman, "Modeling the electromagnetic radiation from electrically small table-top products," *IEEE Trans. Electromagn. Compat.*, vol. 31, pp. 74-84, February 1989.

[6] T. H. Hubing and J. F. Kauffman, "Modeling electrically small, thin surfaces with wire grids," *Applied Computational Electromagnetics Society Journal*, vol. 5, pp. 19-24, Summer 1990.

[7] K. B. Hardin, C. R. Paul, and K. Naishadham, "Direct prediction of common-mode currents," *IEEE Electromagnetic Compatibility Symposium Digest*, pp. 67-71, 1991.

[8] G. Cerri, R. De Leo, and V. M. Primiani, "A rigorous model for radiated emission prediction in PCB circuits," *IEEE Trans. Electromagn. Compat.*, vol. 35, pp. 102-109, February 1993.

[9] T. H. Hubing, "A common problem with printed circuit board radiation models," University of Missour-Rolla Electromagnetic Compatibility Laboratory Technical Report, RF93-3-011P, February 1993. (submitted for publication to the IEEE Trans. Antennas Prop.)

[10] A. E. Ruehli, "Inductance calculations in a complex integrated circuit environment, " *IBM J. Research and Development*, vol. 16, pp. 470-481, 1972.

[11] G. J. Burke and A. J. Poggio, *Numerical Electromagnetics Code (NEC) - Method of Moments*, Lawrence Livermore National Laboratory, January 1981.

[12] H. W. Ott, *Noise Reduction Techniques in Electronic Systems, second ed.*, Wiley-Interscience, New York, 1988.

[13] C. A. Balanis, *Antenna Theory: Analysis and Design*, Harper and Row, New York, 1982.

[14] C. R. Paul, "The concept of dominant effect in EMC," *IEEE Trans. Electromagn. Compat.*, vol. 34, pp. 363-367, August 1992.

6 Appendix : Partial Inductance

Partial Inductance

In the text of this report, the inductance responsible for the voltage drop that induces common mode currents in the current driven case is called a *partial inductance* or a *mutual inductance*. Both of these terms are appropriate in this case, because even though it is a mutual inductance that results in common-mode current, in most practical situations the value of this mutual inductance will be nearly equal to the more-intuitive partial inductance. The purpose of this appendix is to define and describe the term partial inductance as it relates to the models introduced in the report.

Despite the fact that textbooks and sales literature often provide inductance values for isolated current conductors such as printed circuit board traces or braided ground straps, inductance is a quantity that is only defined for current loops. A circuit containing 10 cm of ground strap that has a nominal inductance of 15 nH/cm may have considerably more or considerably less than 150 nH of total inductance.

Current flowing in a conductor produces a magnetic flux that encircles the conductor. The self inductance of a current loop is the net magnetic flux due to the current in a loop that passes through the loop divided by the amplitude of the current. The mutual inductance between two current loops is the net magnetic flux due to the current in one loop that passes through the other loop divided by the amplitude of the first loop's current. Both self and mutual inductance are functions of the loop geometry and (except when nonlinear materials are involved) are independent of the current amplitude.

The tendency for electrical engineers to want to assign values of inductance to parts of a loop without defining the entire loop stems from a desire to quantify the contribution each part will make to the total inductance. This makes it easier to identify which parts of a circuit should be modified in order to most effectively change the overall inductance. It also facilitates analysis of the circuit's behavior using lumped circuit elements. Lumped element circuits are generally more intuitive to electrical engineers and they permit the circuit analysis to be done in terms of scalar voltages and currents rather than vector field quantities.

The inductances defined in textbooks for isolated conductors are normally based on typical current return paths distant from the conductor relative to the dimensions of the conductor cross-section. These estimates of the inductance rely on the fact that the inductance is a relatively weak function of the spacing between conductors in this situation.

In this report, our desire to assign inductances to each piece of a circuit was motivated by a need to quantify the total voltage developed between any two points on the circuit. One must be careful when applying the concept of voltage or a potential difference in the presence of time-varying magnetic fields. The potential difference between two points in a time-varying magnetic field is a function of the path assumed between

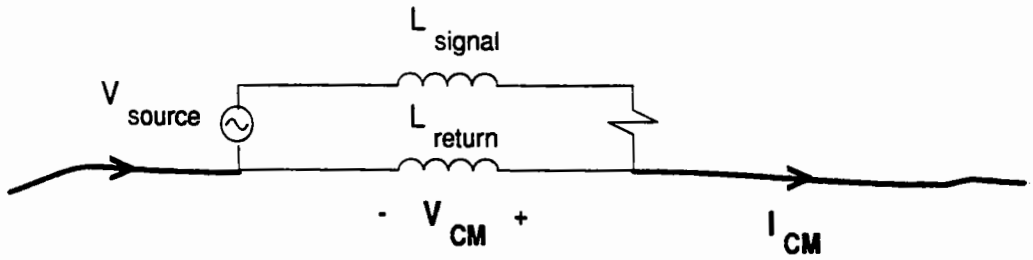

Figure A1: A simple common mode current source

those two points. In our case, we are interested in the voltage that is available to drive common-mode currents onto conductors that are not part of the intended circuit path. In other words, referring to the simple circuit in Figure A1, we would like to define the *partial inductance* of the return conductor such that the common-mode voltage is given by,

$V_{CM} = L\, \delta i/\delta t.$

Self partial inductance and mutual partial inductance

Ruehli [A1], developed the concept of a self partial inductance that could be defined for a given segment of a loop independent of the location or orientation of any other loop segment. For a straight wire segment with a finite wire radius as shown in Figure A2, a nominal rectangular loop is defined that is bounded by the

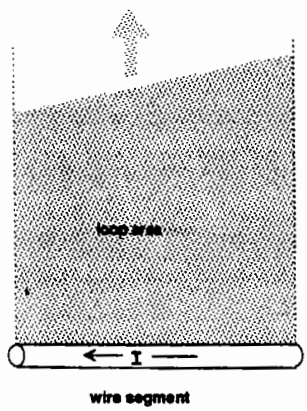

Figure A2: Loop area used to define self partial inductance

wire segment on one side and infinity on the other side. Two lines perpendicular to the wire segment and extending from the ends of the segment to infinity form the other two sides of the loop. The self partial inductance is the ratio of the net flux passing through this loop to the current on the wire segment (in the absence of all other segments and currents).

Ruehli also defined a mutual partial inductance existing between two wire segments. Mutual partial inductance can be viewed as the net flux from one segment that passes through a second segment's infinite rectangular loop divided by the current in the first segment. Referring to Figure A3, it is clear that for two parallel segments the quantity L_{11}-L_{12} (i.e. the self partial inductance minus the mutual partial inductance) is equal to the total flux coupling the loop due to segment 1 divided by the current in segment 1. In other words, L_{11}-L_{12} is the part of the loop inductance due to segment 1. In general, we can define the partial inductance of a segment i to be its self inductance plus or minus the mutual inductances between segment i and all other loop segments,

$$L_i = L_{ii} \pm \sum_{\substack{j=1 \\ j \neq i}}^{n} L_{ij} \quad .$$

Whether the mutual inductance is added or subtracted is determined by the relative orientation of the current on the two segments. If the flux from both segments passes through the infinite rectangular loop area in the same direction, the sign is positive. For segments with current flowing in opposite directions as shown in

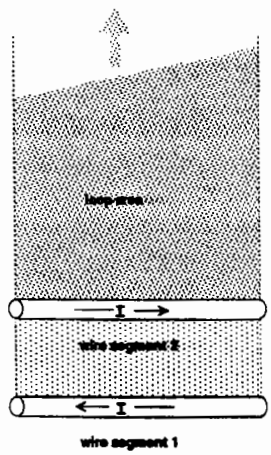

Figure A3: Loop area defining mutual partial inductance

Figure A3, the sign is negative. By defining partial inductance in this manner, the total loop inductance is conveniently expressed as the sum of all the partial inductances,

$$L_{loop} = \sum_{i=1}^{n} L_i \quad .$$

Common mode potential

A voltage drop ($V = L\delta i/\delta t$) can be calculated across each partial inductance and the sum of the voltages must satisfy Kirchoff's voltage law. If we add additional wire segments to form additional current paths it is tempting to apply circuit theory concepts to calculate the currents induced in the new loops. While it is possible to do this, it is important to realize that each additional current carrying segment potentially affects the partial inductance of every other segment. Therefore, in general, the application of the concept of partial inductance still requires a knowledge of all possible current paths.

For our application (i.e. predicting common mode currents), the path of the common-mode current is often unknown and unpredictable. Fortunately, there is one aspect of the common-mode current problem which allows us to use the concept of partial inductance to our full advantage. Partial inductance is usually only important to us in the *current driven* case. The current driven case is associated with relatively low impedance circuits. Common mode current paths on the other hand, have a relatively high impedance. In most cases, the common mode currents are several orders of magnitude smaller than the circuit currents. This means that conductor segments that carry only common mode currents have a relatively small effect on the partial inductance of the circuit segments. Therefore, provided the common mode impedance is high, the common mode potential, V_{CM}, can be calculated solely on the basis of the circuit configuration without a detailed knowledge of the common mode current path.

Conductors of arbitrary cross-section

Ruehli's definition of partial inductance assumes that the current is uniformly distributed on the surface of a thin wire filament. In order to calculate the partial inductance of other conductor shapes, these conductors must be viewed as being composed of many thin filaments. For example, a wide, flat printed circuit board trace might be modeled as several filaments side by side as shown in Figure A4. Analysis of the circuit containing this trace would require all of these filaments and their self and mutual partial inductances to be accounted for. This type of analysis is readily handled using computer techniques, but it is also helpful to have a more intuitive feel for the effect that different conductor shapes have on the partial inductance.

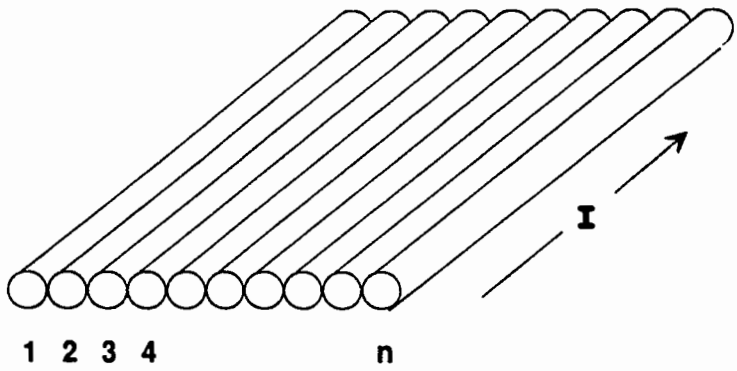

Figure A4: Wide trace modeled with wire filaments

Consider the wide flat trace in Figure A4. The partial inductance associated with each filament is the self partial inductance of that filament plus the mutual partial inductance between that filament and all the other filaments in the trace minus the partial inductance of that filament with the other parts of the loop,

$$L_{filament} = L_{ii} + \sum_{\substack{j=1 \\ j \neq i}}^{n} L_{ij} \pm \sum_{j=n+1}^{m} L_{ij} \quad .$$

Since the filaments in the same trace are tightly coupled, their mutual partial inductances will be high (but still less than the self partial inductance). Therefore, the partial inductance of each filament will be nearly n times greater when it is located near the other filaments than it would be if it were isolated from the others. However, the partial inductance of the wide trace overall is actually the parallel combination of all of the filament partial inductances. Assuming each filament had approximately the same partial inductance, the trace partial inductance would be the filament partial inductance divided by n. Widening the trace, lowers the partial inductance because the additional parallel inductance more than compensates for the added self inductance of each filament.

A computer analysis of this configuration would also show that the self partial inductance of the outer filaments is slightly lower than that of the inner filaments. As a result, more of the current flows on the outside edge of the trace.

Reference

[A1] A.E. Ruehli, "Inductance calculations in a complex integrated circuit environment," *IBM J. Res. Develop.*, vol. 16, no. 5, pp. 470-481, Sept. 1972.